frontiers in Materials

REVIEW
published: 06 February 2020
doi: 10.3389/fmats.2020.00018

A Remarkable Class of Nanocomposites: Aerogel Supported Bimetallic Nanoparticles

Hande Gunes[1], *Yaprak Özbakir*[2], *S. Bengisu Barim*[1], *Hamed Yousefzadeh*[1], *Selmi E. Bozbag*[1] *and Can Erkey*[1]*

[1] Department of Chemical and Biological Engineering, Koç University, Istanbul, Turkey, [2] Department of Chemical and Biological Engineering, Üsküdar University, Istanbul, Turkey

Aerogels are a unique class of materials due to their low density, high porosity, high surface area, and an open and interconnected pore structure. Aerogels can be organic, inorganic and hybrid with a plethora of surface chemistries. Aerogel-based products for thermal insulation are already in the market and many studies are being conducted in many laboratories around the world to develop aerogel-based products for other applications including catalysis, adsorption, separations, and drug delivery. On the other hand, bimetallic nanoparticles dispersed on high surface area carriers, which have superior properties compared to their monometallic counterparts, are used or are in development for a wide variety of applications in catalysis, optics, sensing, detection, and medicine. Investigations on using aerogels as high surface area carriers for dispersing bimetallic nanoparticles are leading to development of new composite materials with outstanding properties due to the remarkable properties of aerogels. The review focuses on the techniques to synthesize these materials, their properties, the techniques to tune their pore properties and surface chemistry and the applications of these materials.

Keywords: aerogel, nanocomposite, support, nanoparticles, bimetallic, mesoporous

OPEN ACCESS

Edited by:
Ying Zhou,
Southwest Petroleum University, China

Reviewed by:
Vladimir Ivanov,
N.S. Kurnakova Institute of General and Inorganic Chemistry (RAS), Russia
Junzong Feng,
National University of Defense Technology, China

***Correspondence:**
Can Erkey
cerkey@ku.edu.tr

Specialty section:
This article was submitted to Polymeric and Composite Materials, a section of the journal Frontiers in Materials

Received: *25 October 2019*
Accepted: *16 January 2020*
Published: *06 February 2020*

Citation:
Gunes H, Özbakir Y, Barim SB, Yousefzadeh H, Bozbag SE and Erkey C (2020) A Remarkable Class of Nanocomposites: Aerogel Supported Bimetallic Nanoparticles. Front. Mater. 7:18. doi: 10.3389/fmats.2020.00018

INTRODUCTION

Aerogels

A wide variety of aerogels were first synthesized in 1931 (Kistler, 1931) by replacing the liquid part of a gel with air without collapsing the gel. Aerogels are generally considered as materials with low densities, high surface areas and high porosities. Since the development and commercialization of silica aerogel-based blankets for thermal insulation, the number of studies that are being conducted at many laboratories around the world on using aerogels for applications other than insulation is growing at an accelerating pace. Aerogels can be organic (e.g., starch aerogel, STA, alginate aerogel, ALA, resorcinol formaldehyde aerogel, RFA), or inorganic (e.g., silica aerogel, SA; alumina aerogel, AA; titania aerogel, TA) (Pierre and Pajonk, 2002). Carbon aerogels (CAs) is another class of aerogels obtained by pyrolysis of organic aerogels. Aerogels have particularly attractive properties as adsorbents, catalysts, and drug delivery devices. The properties of aerogels can further be enhanced by making composites of aerogels with other materials, such as polymers (Sanli and Erkey, 2013), fibers, and metallic nanoparticles (NPs) (Vallribera and Molins, 2008). Among these, a wide variety of aerogel supported monometallic NPs have been developed for various applications. For instance, Pt/CA (Barim et al., 2017), Pt/graphene aerogel (GA) (Sarac Oztuna et al., 2017), N-doped Co/CA and Fe/CA (Sarapuu et al., 2015) were synthesized and tested as

electrocatalysts for oxygen reduction reaction (ORR). Cu/CA (Han et al., 2019) was utilized for CO_2 reduction reaction and Pt/CAs were investigated for proton exchange membrane fuel cell (Smirnova et al., 2005) and direct methanol fuel cell (DMFC) (Wei et al., 2009) applications. TiO_2/CA was investigated as a photoelectrocatalyst for wastewater treatment (Jin et al., 2011). Ni/CA and Fe/CA were used as ammonia adsorption catalysts for gas purification (Gómez-Cápiro et al., 2018). SnO_2/GA was used as a NO_2 gas sensor (Liu et al., 2014; Li et al., 2015). Ag-AgBr/TiO_2/GA was used for photocatalytic destruction of organic dyes and bacteria (Zhang et al., 2019). Recently, the emphasis has shifted to aerogel supported bimetallic NPs which have superior properties than their monometallic counterparts due to a wide variety of factors including tunable properties by varying composition of metals, higher thermal stability, enhanced metal-support interactions, higher resistance to poisoning and/or coke deposition, prevention of NP growth and higher catalytic activity and selectivity of supported bimetallic NPs compared to monometallic counterparts (Takanabe et al., 2005; Koh et al., 2007; Chen et al., 2010; Yu et al., 2015; Hossain et al., 2017; Zhou et al., 2017; Wang and Zhu, 2018).

This review gives an overview of the advantages and disadvantages of the techniques used to synthesize aerogel supported bimetallic NPs, the properties of these materials as well as their applications. Bimetallic NPs and supported bimetallic NPs, their formation and growth, and their importance in various applications are discussed in section Bimetallic Nanoparticles and Supported Bimetallic Nanoparticles. Advantages of aerogels as support materials are explained in section Advantages of Aerogel Supported Bimetallic Nanoparticles. Synthesis routes and material properties of aerogel supported bimetallic NPs are given in section Synthesis and Properties of Aerogel Supported Bimetallic Nanoparticles. Their applications in catalysis, optics and sensors are given in section Applications. The research needs for further development and commercialization of these materials are discussed in section Conclusions and Future Directions.

Bimetallic Nanoparticles and Supported Bimetallic Nanoparticles

Bimetallic NPs are composed of two different metals. Bimetallic NPs are of both academic and industrial interest as their properties are often different from either of the two pure NPs. Similar to bulk alloys, bimetallic NPs exhibit a very wide range of combinations and compositions. Bimetallic NPs (A_mB_n) can be generated with more or less controlled amount (m + n) and composition (m/n) with main mixing patterns given in **Figure 1**.

The formation and growth of single component NPs usually consist of a number of steps including nucleation, diffusion and growth. All these steps are usually governed by kinetic phenomena (Mondloch et al., 2012). The degree of segregation/mixing and atomic ordering in A_mB_n bimetallic NPs depends on a variety of factors including relative strengths of A-A, B-B, and A-B bonds, relative surface energies of bulk A and B, relative atomic sizes, strength of binding to surface ligands (or surfactants) and specific electronic/magnetic effects

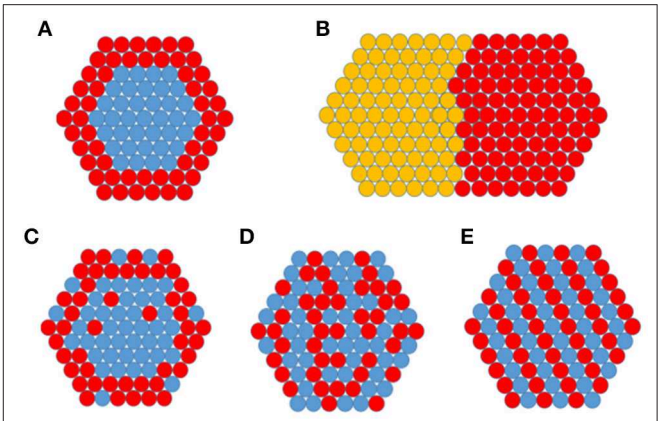

FIGURE 1 | Schematic representation of the examples of some possible configurations for bimetallic NPs: **(A)** core-shell, **(B)** segregated/Janus particle, **(C)** surface segregated, **(D)** disordered alloy, **(E)** ordered alloy. The illustrations display cross sections of the NPs showing an hypothetical face-centered cubic (FCC) (111) plane.

(Ferrando et al., 2008). The structure of the NP and degree of A-B segregation may also depend on kinetics of nucleation and growth for which the method and conditions of NP generation (type of particle source, metal precursor (MP), support, surfactant, temperature, pressure, etc.) becomes important.

The knowledge on the phase behavior of the alloys is important. Although the phase diagrams of bulk alloy systems have been extensively reported, their extension to the nanometer sized regime is not trivial since the perturbations in both morphology and electron density due to finite sizes at nanoscale can give rise to non-bulk like properties (Oviedo and Leiva, 2013). For instance, pairs of elements, such as FeAg (Ferrando et al., 2008) or AuPt (Wanjala et al., 2010) have large miscibility gaps in bulk crystalline state but can mix as NPs. PtRu bimetallic NPs with 1.5 nm diameter and with a Pt:Ru ratio of 0.2 display an FCC closed-packed crystal structure whereas bulk alloy of the same species with the same composition exhibit a hexagonal-closed packed (HCP) structure (Michael S. Nashner et al., 1997). These observations point out that a divergence may exist between the structural properties predicted by the bulk phase diagrams and those displayed by metal NPs.

Supported NPs are NPs which are dispersed on the surface of highly porous substrates or films (Eppler et al., 1997). Because of their high surface energy and intrinsic instability, NPs tend to form agglomerates which diminish their desirable properties. Therefore, supports with high surface areas are often used to serve as carriers and stabilizers. Supports also prevent the oxidation of NPs to some extent. Thus, the intrinsic properties and morphologies of NPs are conserved depending on the support-metal interaction or support topology. Supported NPs are used in a number of technologically important areas, ranging from catalysis (e.g., catalytic converters in automobiles and electrochemical fuel cells) to optics, electronic, magnetic, and medical applications (Kitchin et al., 2004). In catalysis, supports have a crucial role in the transport of the reactants and products to and from the active sites (Antolini, 2009) and in some

cases they may participate in the catalytic reactions as well (Vanrysselberghe and Froment, 1996; Deka et al., 2013).

In catalysis, supported bimetallic NPs are used to enhance the performance and for economic reasons (Sankar et al., 2012). The activity of bimetallic NPs depends on the metal concentration, morphology, and atomic ordering. In alloy NPs, the intrinsic catalytic activity adjustment originates from two cumulative phenomena called the ligand and the strain effect. The addition of another metal causing alteration in the electron density of the system (ligand effect) and the metal-metal bond length change (strain effect) may lead to improved catalytic activity (Kitchin et al., 2004; Bosco et al., 2009). The incorporation of a second metal into the structure may also prevent the poisoning of the catalyst and prolong its aging behavior (Winkler et al., 2010; Wiebenga et al., 2012). Since catalytic reactions occur only at catalytic sites residing on the surface of NPs, a significant proportion of the atoms are effectively wasted in the catalytic process. This is particularly important for expensive catalyst metals, such as Pd and Pt (Ghosh Chaudhuri and Paria, 2012). In order to reduce costs, there is, therefore, considerable interest in synthesizing A-B core-shell NP catalysts, where A is a relatively inexpensive metal (e.g., Co, Ni, Cu), which is (generally) less catalytically active residing at the core, and B is a more expensive, more catalytically active metal (typically Pd or Pt) residing at the shell. Synergetic electronic effects toward catalytic reactions can also be significant in alloy or core-shell NPs via the introduction of a change in the d-band center of the metal via the addition of second metal (Greeley and Nørskov, 2005; Koh and Strasser, 2007). Good examples of these phenomena are highest intrinsic activity of Pt_3Ni (Stamenkovic et al., 2007) and dealloyed $PtCu_3$ (Mani et al., 2008) as compared to pure Pt toward the ORR.

Bimetallic NPs, in particular, core-shell NPs, have very special optical properties that can be tuned with structural and compositional modification. The relative modification of core and shell radii produces spectral shifts in a wide range that is in some cases as important as the morphological changes in a single component NP along with some possible applications in Surface Enhanced Raman Spectroscopy (SERS) (Negre and Sánchez, 2013).

Advantages of Aerogel Supported Bimetallic Nanoparticles

Aerogels as supports have many advantages compared to conventional porous materials used as supports for bimetallic NPs. The pore size of aerogels can be adjusted by changing synthesis conditions (Pekala, 1989). Moreover, aerogels have also a very narrow pore size distribution. Both of these factors may enable better control over the rates of diffusion of reactants and products to and from catalytic sites consisting of bimetallic NPs leading to higher conversions or selectivities in a particular reactor. Moreover, combination of powerful sol-gel chemistry with new techniques, such as supercritical deposition to prepare supported bimetallic NPs are leading to development of aerogel supported materials with superior properties (Barim et al., 2018). Unlike conventional porous materials, aerogels can also be produced in any form, such as beads, cylinders and monoliths which may be advantageous for various applications, such as optofluidic microreactors (Özbakir et al., 2017). There are also aerogels which are organic-inorganic hybrids with very complex morphologies which may be beneficial in designing systems for a wide range of reasons, such as to reduce deactivation rates or improve stability of bimetallic NPs (Kanamori et al., 2007, 2008; Hayase et al., 2014).

SYNTHESIS AND PROPERTIES OF AEROGEL SUPPORTED BIMETALLIC NANOPARTICLES

Routes to synthesize aerogel supported bimetallic NP synthesis are similar to the ones for conventionally supported bimetallic NPs (Vallribera and Molins, 2008). They can either be formed by deposition of the MPs on the pre-synthesized aerogel support, or by synthesis of the aerogel support along with the deposition of metal NPs or MPs; followed by the conversion of MPs to NPs. The most commonly used methods include sol-gel method, liquid phase impregnation, supercritical deposition, microwave-assisted deposition and electroplating. Their advantages and disadvantages; along with literature examples are summarized in **Table 1**. The routes and properties of prepared nanocomposites are explained in detail in the following subsections.

Sol-Gel Route

Sol-gel method is a simple and widely used technique to prepare aerogel supported bimetallic NPs under mild experimental conditions (Liu et al., 2013, 2015; Herrmann et al., 2014; Rechberger and Niederberger, 2017; Wen and Eychmüller, 2017). The method is based on polymerization chemistry which enables evolution from a molecular state to a continuous network via hydrolysis and polycondensation reactions (Schubert, 1996). Different strategies to synthesize inorganic aerogel supported bimetallic NPs have been developed using the sol-gel route (Mörke et al., 1994; Vallribera and Molins, 2008; Corrias and Casula, 2011) which consist of following steps: hydrolysis, introduction of the metals as precursors or NPs, condensation/gelation, solvent exchange, drying and thermal or chemical treatment of gels in order to convert MPs to their metal forms. Depending on the addition step of the metal (before or after hydrolysis) or the form of metal introduced (either as NPs or as MPs), four different routes are possible as shown in **Figure 2**. In the first route (Route A in **Figure 2**), MP solutions are mixed with skeleton precursor solution prior to hydrolysis. Multicomponent sol then undergoes condensation/gelation. After gelation, MPs are trapped inside the gel (Mörke et al., 1994). Subsequently, solvent exchange and supercritical drying are applied. Afterwards, MPs are converted to bimetallic NPs via thermal treatment or reduction by hydrogen, depending on the precursor properties. Hydrogen treatment at high temperatures (e.g., 300-800°C) can be applied to transform the bimetallic NPs into alloy NPs (Heinrichs et al., 1997; Job et al., 2005; Lambert et al., 2005). Alternatively, MPs can be introduced to the sol after hydrolysis of skeleton precursor (Route B in **Figure 2**). Resulting multicomponent sol undergoes condensation/gelation reactions,

TABLE 1 | Advantage and disadvantages of aerogel supported bimetallic nanoparticle synthesis methods.

Method	Synthesized Nanocomposites		Advantages	Disadvantages
Sol–Gel	PdAg/SA FeCo/SA FeMo/SA FeCo/AA RuNi/AA CoNi/AA	AuAg/TA PdRu/CA CoNi/CA PdNi/CA PtPd/GA	- Simple procedure with well-defined steps - Enables good control of loading and composition	- Presence of metallic precursors may change polymerization pathways - Pre-formed NP aggregation or sedimentation may hinder homogeneous dispersion within the gels
Liquid phase impregnation	PtNi/CA PtRu/CA PtCu/SA		- Simple procedure with well-defined steps - Straightforward control of metal loading, therefore suitable for deposition of expensive metals	- Evaporation of solvent or reduction of precursors may result in agglomerates of metal NPs - Size control is difficult due to slow diffusion of ions through liquid solvent - High surface tension of liquid solvents may result in pore collapse of aerogels - Usually nitrate salts of metals are used as precursors
Supercritical deposition	PtCu/CA PtFe/GA		- Fast deposition, rapid penetration and wetting of pores due to enhanced mass transfer rates - Prevention of pore collapse of aerogels due to the lack of a liquid phase - Easy control over metal loading, particle size and distribution - High conversion rate of MPs due to complete miscibility of reactant gases in SCFs	- Requirement of SCF-soluble MPs, which are generally expensive - Limitation of maximum metal loading in accordance with MP solubility in SCF and affinity of MP with the support
Microwave-assisted deposition	PtCu/SA PtAu/CA		- Relatively fast route compared to aforementioned methods	- Agglomerates of NPs may be formed due to hot spots during microwave treatment
Electroplating	FeCoP/GA		- Simple and conventional route to prepare good candidates of metal/support composites for electrocatalysis applications	- Not suitable for inorganic support decoration due to the usage of electrodes

solvent exchange, supercritical drying and conversion of MPs to bimetallic NPs, as in Route A.

Another technique of producing aerogel supported bimetallic NPs is the utilization pre-formed colloidal NPs, which are synthesized via reduction of MPs in a solution by the help of a reducing agent with or without stabilizing agents, depending on precursor and reducing agent properties (Reetz, 2007). Colloidal NPs can be introduced to the sol either before (Route C in **Figure 2**) or after (Route D in **Figure 2**) hydrolysis (Vallribera and Molins, 2008; Sadrieyeh and Malekfar, 2018a,b; Tesfaye et al., 2019). A similar procedure to Route C was reported by Da Silva et al. (2015) for Pt/rGO/TA (Pt multilayer reduced graphene oxide TA) synthesis. However, it has not yet been applied to aerogel supported bimetallic NPs to our knowledge. Since metals are already introduced as NPs in these routes, thermal treatment or chemical reduction is not necessary after drying step.

Among a broad range of inorganic aerogels, SA has been extensively investigated due to its well-developed sol-gel chemistry. PdAg/SA catalyst for selective dehydroclorination of 1,2-dichloroethane to ethylene was prepared via Route B using tetraethyl orthosilicate (TEOS), and palladium(II) acetyl acetonate and silver acetate, followed by supercritical drying, calcination and reduction with H_2 (Heinrichs et al., 1997). TEM images demonstrated that aerogels were decorated with small and large alloy NPs with diamaters ranging from 2 to 3 and 7 to 10 nm. Magnetic FeCo/SA was synthesized through Route A using TEOS, iron(III) nitrate and cobalt(II) nitrate, and an acid catalyst followed by high temperature supercritical drying and thermal treatment with H_2 at 800°C (Casula et al., 2002, 2003). The procedure resulted in formation of homogenously dispersed spherical FeCo alloy NPs with ∼10 nm in size within the porous SA matrix with a high surface area of ∼800 m^2/g. The same group later demonstrated that urea-assisted co-gelation of silica and MPs led to fast gelation in preparation of FeCo/SA. The alloy NPs were 2-3 nm in size and homogeneously distributed in the pores of SA after a prolonged heat treatment (Casula et al., 2007; Casu et al., 2008). This route was then adapted for the synthesis of FeMo/SA (Marras et al., 2015). Fe and Mo NP sizes were in the range of 4-10 and 15 nm, respectively, however, alloy formation was not addressed.

AA was also used as a support for bimetallic NPs. FeCo/AA was prepared using Route B based on pre-hydrolysis of aluminum precursor, aluminum tri-sec-butoxide, subsequent co-gelation with iron(III) nitrate and cobalt(II) nitrate followed by high temperature supercritical drying and a reduction treatment (Corrias et al., 2004; Casula et al., 2005). Nanocomposites with overall alloy loading of 10 wt%, high surface area (300 m^2/g) and low density (∼0.03 g/cm^3) were obtained. RuNi/AA was prepared via Route A, using aluminum isopropoxide as the skeleton precursor with nickel(II) nitrate and ruthenium(III) acetyl acetonate (Hossain et al., 2017). The gel was dried

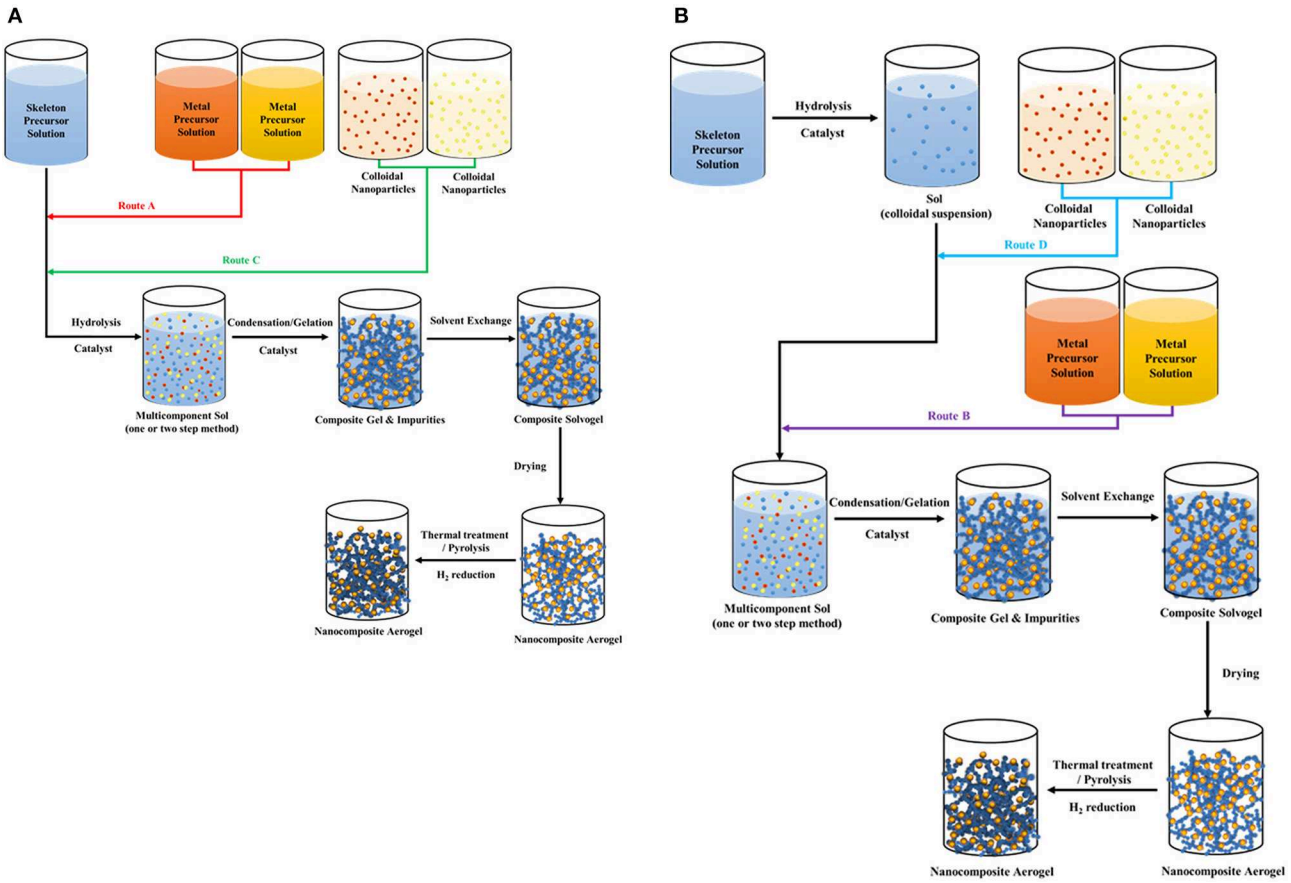

FIGURE 2 | Schematic of preparation of aerogel supported bimetallic NPs via sol-gel method with the addition of MPs (Route A and B) or metal NPs (Route C and D) **(A)** before hydrolysis and **(B)** after hydrolysis.

by supercritical drying, then calcined and heated under H_2 flow to promote the alloy formation in the alumina matrix. Average NP size was found to be 7.9 nm. BET surface area was 380 m^2/g and pore volume was found to be 0.75 cm^3/g. XRD and H_2-TPR results indicated the formation of RuNi alloy formation. Co/AA and CoNi/AA were synthesized via Route B, using aluminum nitrate as skeleton precursor, and cobalt(II) nitrate and nickel(II) nitrate as MPs. After gelation followed by supercritical ethanol drying at 260°C and 8.0 MPa, a composite powder was formed (Chen et al., 2010). Then, the sample was calcined at 650°C for 4 h in air. The average size of CoNi alloy NPs was 17 nm, while the average NP size of Co/AA was 25 nm. Also, the BET surface area of bimetallic aerogel (207.8 m^2/g) was more than the monometallic Co/AA (170 m^2/g).

AuAg/TAs were synthesized using Route D (Sadrieyeh and Malekfar, 2018a). The pre-synthesized Au and Ag NPs were added to a titania sol which was prepared with titanium isopropoxide. After gelation, solvent exchange, and supercritical drying steps, AuAg/TA was obtained. TEM results showed that uniform dispersion could not be obtained. Size of NPs varied between 6.5 and 7.5 nm.

CAs are mesoporous materials with enriched porosity and high specific surface areas, making them favorable for many practical applications (Thirumalraj et al., 2018; Tesfaye et al., 2019). They are generally produced by pyrolysis of organic aerogels. PdRu/CA was prepared via dropwise addition of palladium(II) chloride and ruthenium(III) chloride to phloroglucinol-formaldehyde (PhI-F) sol (Thirumalraj et al., 2018). Following gelation, curing, carbonization, and drying steps, PdRu alloy NPs with particle size ranging from 50 to 100 nm were homogeneously distributed on the surface of the CA matrix. Recently, CoNi/CA was prepared by first mixing sodium alginate solution with a salt solution to form granular hydrogel, followed by freeze-drying, annealing, and carbonization (Xie et al., 2019). NPs with diameters ranging from 10 to 20 nm were uniformly dispersed. CoNi alloy NPs with a core-shell hierarchical structure covered with graphitized carbon materials were observed in TEM images. NiCo/MWCNT (multiwalled carbon nanotube) was fabricated by a polyol reduction method starting with nickel(II) chloride and cobalt(II) chloride (Tesfaye et al., 2019). NiCo/MWCNT/PVAA (polyvinyl alcohol aerogel) was produced by mixing PVA solution with NiCo/MWCNT powder and freeze drying of the resulting hydrogels. Ni and

Co NPs were uniformly distributed. When Co:Ni ratio was >0.25, agglomeration and growth of Co crystals started to occur. For smaller Co:Ni ratios, presence of Co decreased NP size. N and S doped PdNi/CA was prepared by adding raw cotton into palladium(II) chloride and nickel(II) acetate solution (Raj kumar et al., 2019). After hydrothermal treatment with thiourea, PdNi anchored carbon fiber hydrogels doped with N and S were obtained. XRD and SAED patterns confirmed that highly crystalline PdNi NPs were formed on N, S doped CA.

GAs are a class of carbon aerogels produced from layers of graphene. PtPd/GA on Ni foam (NF) were prepared using potassium hexachloroplatinate(IV) and potassium hexachloropalladate(IV) as MPs (Tsang and Leung, 2017, 2018; Tsang et al., 2017, 2019). MPs were added to a solution of graphene oxide (GO) dispersed in water and mixed. NF strip was added to the solution with ultrasonic treatment for 20 min and then kept at room temperature for 2 h. Vitamin C was added to the solution to form bimetallic NPs. PtPd/GH/NF (PtPd graphene hydrogel on NF) was obtained after thermal treatment at 60°C for 48 h. Afterwards, PtPd/GA/NF was obtained by freeze drying. TEM images showed that PtPd NPs had irregular shapes and were significantly larger than those in other studies involving GAs. The agglomeration of metal NPs was attributed to the absence of continuous stirring during formation of PtPd/GA network on NF. TEM, EDX and XRD analyses indicated PtPd alloy formation.

The presence of metallic precursors used in sol-gel route may cause undesirable pore properties since they may adversely affect the polymerization pathways (Bozbag and Erkey, 2015). Although it is a simple route and enables a good control of loading and composition, the aggregation and/or sedimentation of the pre-formed NPs may hinder the development of a homogenous dispersion in the gels. This can be overcome by functionalization of the surface of the NPs before gelation. Soft sonication may prevent sedimentation of the NPs during this stage (Hund et al., 2004; Vallribera and Molins, 2008).

Liquid Phase Impregnation

In liquid phase impregnation technique, a solution of MP is contacted with the support followed by filtering, drying and reduction steps. Wet impregnation and incipient wetness impregnation are two types of liquid impregnation based on the amount of solution used. If the volume of precursor solution used for impregnation is more than total pore volume of the support, the method is called wet impregnation. If the volume of the precursor solution is precisely equal to the pore volume of the support, then the technique is called incipient wetness, or dry impregnation method. Filtration step is not required for incipient wetness method. It is necessary to apply thermal treatment in a calcining and/or reducing environment in order to remove the anions (Pinna, 1998; Mehrabadi et al., 2017). In wet impregnation, the MP solution is contacted with support for a desired time and then the mixture is washed, filtered, and dried. MPs could potentially adsorb chemically and/or physically on the support. Physically adsorbed molecules may be removed during washing, filtration, and drying steps. Initial concentration of the precursor, temperature, pH of the solution, support pore volume and its surface chemistry are the important factors affecting the loading of the MPs on the support (Pinna, 1998). Surface oxygen containing groups, such as hydroxyl in inorganic oxide supports and surface oxygenated groups in carbonaceous supports determine the charge of support surface which play an important role in binding the oppositely charged MPs with surface ionic sites. The pH of aqueous solutions can change the surface charge of the supports since the surface oxygen containing groups react either with protons or hydroxyl groups in the solution. Therefore, pH and precursor concentration should be tuned accordingly.

Both wet and dry impregnation routes can be carried out via simultaneous or sequential impregnation of metals. In simultaneous impregnation, both MP solutions are mixed with support at the same time, followed by the subsequent steps of impregnation. In sequential impregnation, one of the MP solution is added to the support and treated as in the preparation of supported monometallic NPs. Subsequent to the preparation of supported monometallic NPs, the second MP solution is added to the prepared composite and then the subsequent steps of impregnation are applied.

PtNi/MWCNT-GA was prepared via simultaneous wet impregnation (Wang et al., 2017b). GO was synthesized via Hummer route. Two mixtures of the synthesized GO and MWCNT were prepared and sonicated. A precursor solution containing platinum(IV) chloride, nickel(II) chloride, sodium glutamate and 10 mL of EG solution containing 0.5 M NaOH was added to the GO and MWCNT suspension and stirred for 30 min. Then the mixture was maintained at 200°C for 10 h to form a cylindrical foam followed by washing, freeze drying and heat treatment at 450°C under N_2/H_2 gas mixture to obtain PtNi/MWCNT-GA. XRD of the prepared sample did not show any metallic Ni or Ni-oxide peaks indicating that Ni atoms were successfully incorporated into the Pt lattice as evident from the contraction in the lattice parameter obtained from XRD and TEM. Despite a substantially high PtNi metal loading of 80%, authors reported that PtNi NPs were distributed homogenously on the aerogel surface with an average PtNi NP size of 15 $\pm$ 1.0 nm showing that porous structure of the aerogel led to high metal dispersion at a very high metal content of 80 wt.% (**Figure 3**). Pt:Ni mole ratio was given as 1:1.05.

PtRu/CA was prepared via simultaneous wet impregnation (Du et al., 2007). CA was ultrasonically mixed with isopropanol and water for 1 h. Then, the resulting slurry was mixed with hexachloroplatinic acid and ruthenium(III) chloride. $NaBH_4$ was used as the reducing agent Then, the catalysts were dried at 75°C in air. Total metal loading was 20 wt%. Prepared CA had a high surface area of 576 m^2/g and a narrow pore size distribution with average pore size of 11.4 nm indicating a highly mesoporous structure. XRD showed that all plane angles were shifted to higher 2θ values showing that PtRu disordered alloy NPs were successfully formed on CA. TEM images showed that PtRu dispersion is better on CA when compared commercial PtRu catalyst on carbon black with slightly higher mean NP size (∼3 nm). Better dispersion was attributed to higher surface area of CA than carbon black.

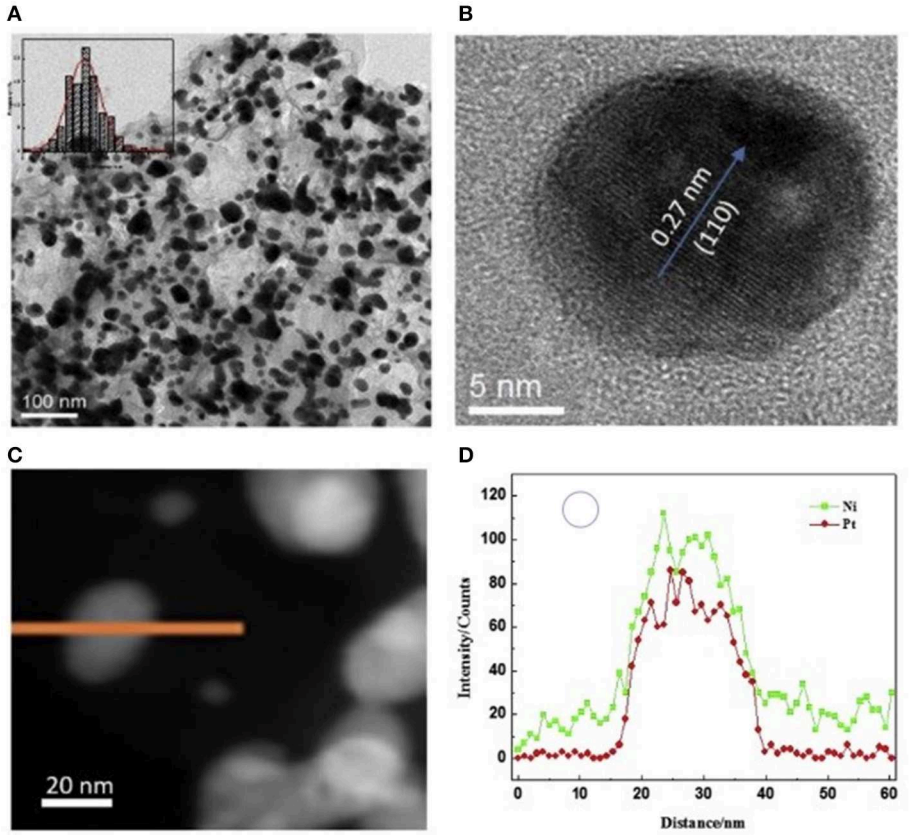

FIGURE 3 | (A) TEM image, and the inset is the particle size distribution of PtNi NPs for PtNi/CA; **(B)** HRTEM image of a single PtNi NP; **(C)** EDS line scan of one PtNi NP and **(D)** Pt, Ni distribution. Reprinted from Wang et al. (2017b), ©2017, with permission from Elsevier.

PtCu/SA was synthesized via sequential wet impregnation (Wang and Zhu, 2018). First, copper(II) nitrate was dissolved in water followed by dropwise addition of ammonia solution to adjust the pH. SA was then added and stirred for 4 h. The blue powder was collected by filtration and washing and then dried at 80°C. Then, the resulting powder was added to the hexachloroplatinic acid ethanol solution followed by stirring, filtering, and drying at 80°C for 12 h to remove the ethanol solvent. Final PtCu/SA was obtained after treatment at 300°C under H_2 flow. The XRD patterns of the PtCu/SA and Pt/SA showed that the peaks of Pt(200) and Pt(220) disappeared in PtCu/SA indicating that the incorporation of Cu to the crystal lattice of Pt. Moreover, the size of Pt particles was decreased, and the dispersion of Pt was improved. Particle size calculations based on the Scherrer equation revealed that the introduction of Cu decreased the Pt particle size from 21.5 nm in Pt/SA to 11.0 nm in PtCu/SA.

Liquid phase impregnation has some disadvantages. Evaporation of the solvent or reduction of inorganic precursors at high temperatures may lead to agglomeration of metal NPs on the support surface. It is difficult to control the size of metal NPs if the pore size distribution is broad. Furthermore, it is difficult to control NP size due to slow diffusion of ions through the liquid solvent. In addition, nanopores of the aerogels could collapse due to high surface tension of the liquid solvents, leading to a reduction in surface area and blockage of pores. As the liquid solvent is removed from the pores during the drying step, meniscus of retreating liquid creates locally strong forces which may lead to collapse of the pores (Bourikas et al., 2006; Erkey, 2009).

Supercritical Deposition

Supercritical deposition (SCD) is a powerful alternative technique for the preparation of supported metallic NPs which was first introduced in 1995 (Watkins and McCarthy, 1995). A supercritical fluid (SCF) is a fluid that has been heated and compressed above its critical temperature and pressure. **Figure 4** shows three major steps of SCD which are dissolution of a MP in a SCF followed by adsorption of the precursor onto the surface of the support and conversion of the precursor to its metal form by various routes (Erkey, 2009; Bozbag et al., 2012; Türk and Erkey, 2018). Simultaneous (Cangül et al., 2009) deposition and sequential (Bayrakçeken et al., 2010) deposition are basically two approaches utilized for the synthesis of supported bimetallic NPs via SCD. In simultaneous SCD, two MPs are dissolved in SCF at the same time and then the subsequent steps of SCD are carried out whereas in sequential SCD, the single component SCD procedure is repeated twice.

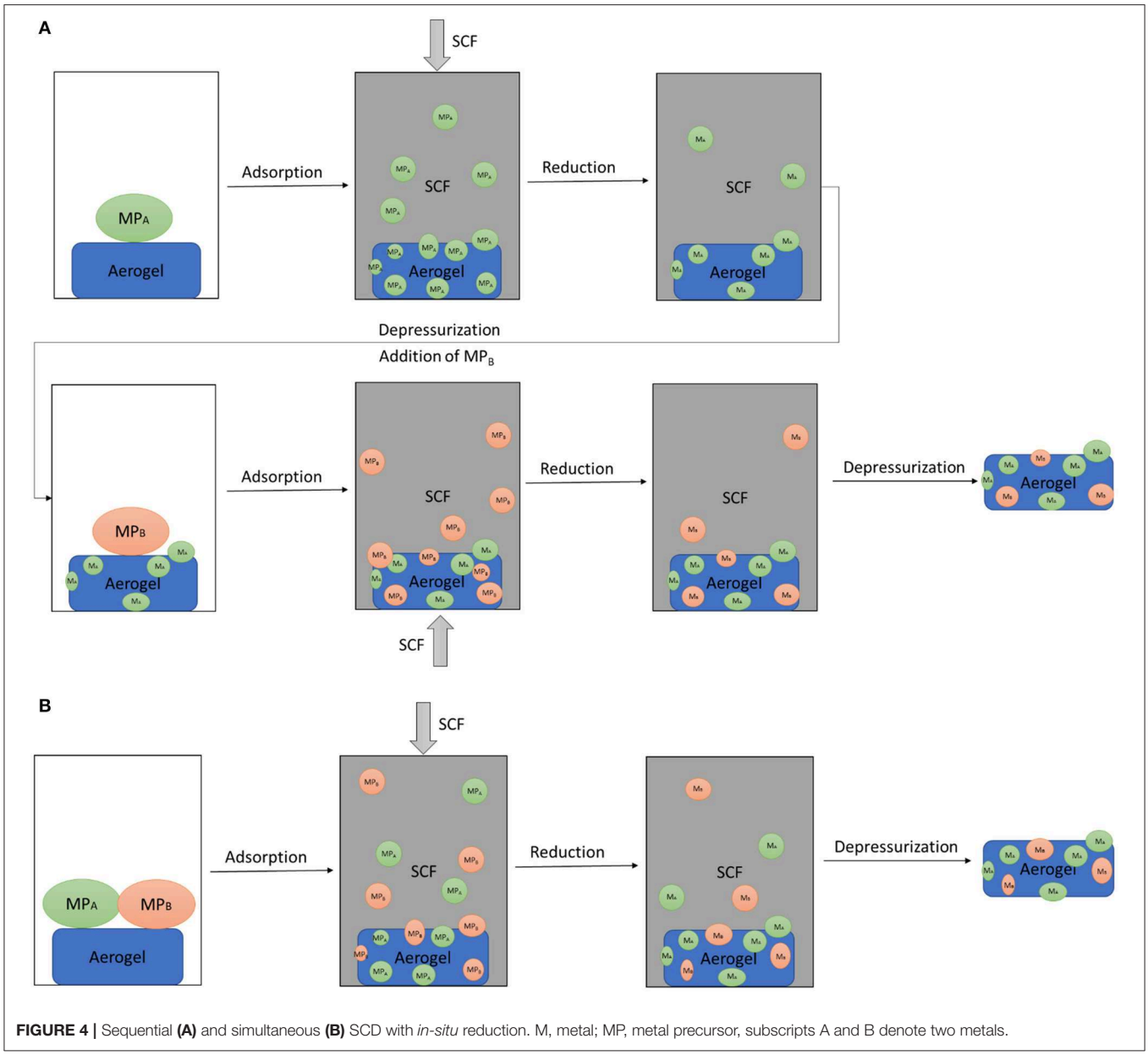

FIGURE 4 | Sequential **(A)** and simultaneous **(B)** SCD with *in-situ* reduction. M, metal; MP, metal precursor, subscripts A and B denote two metals.

Due to gas-like diffusivity and viscosity, mass transfer rates in the presence of a SCF are fast. This enables fast rates of deposition, rapid penetration and wetting of pores as compared to liquid solvents (Zhang et al., 2008). A wide range of MPs can be dissolved in SCFs due to their liquid-like density (Erkey, 2009; Türk and Erkey, 2018). Using SCF as a solvent also prevents the pore collapse that may occur for nanostructured substrates, such as aerogels when organic solvents are used. Adjusting the thermophysical properties of SCFs like temperature and pressure, can be a very useful tool for the synthesis of supported NPs with remarkable control on loading, particle size and distribution. Furthermore, due to complete miscibility of SCFs with reactant gases, such as H_2 and O_2, high concentrations of the reactant gases can be obtained within SCF. This leads to high conversion rates of MPs to their metal forms, given that the reaction is not zeroth order with respect to the reactant gas. CO_2 has been the most commonly used SCF ($scCO_2$) since it is inexpensive, non-toxic, and non-flammable and has relatively easily accessible critical conditions Tc (31.1°C) and Pc (7.38 MPa).

The first study on the preparation of aerogel supported bimetallic NPs using SCD was reported by Erkey's group (Bozbag et al., 2013), who synthesized PtCu/CA using simultaneous SCD in $scCO_2$. In this study, the binary adsorption isotherms of MPs on CAs in a SCF medium were measured for the first time and modeled using the Ideal Adsorbed Solution Theory. The control over bimetallic NP properties, such as metal loading and metal composition was possible through the usage of the binary adsorption isotherms of the MPs. For the synthesis,

bis (1,1,1,3,5,5,6,6,6-nonafluorohexane-2,4 diiminate) copper and dimethyl(1,5-cyclooctadiene)platinum(II) were dissolved in $scCO_2$ and adsorbed on the CAs. The adsorption equilibrium was reached in 4 h depending on the initial concentration of the MPs. Following the adsorption step, the adsorbed MPs on the CAs were thermally converted to their metal form under flowing N_2 at 400°C for 4 h. Prepared nanocomposite was characterized by TEM, XRD, and XPS. TEM images showed a homogeneous dispersion of NPs with a sharp particle size distribution. The size of the particles ranged from 2.9 to 7.2 nm. XRD patterns showed systematic shift in peaks indicating disordered FCC PtCu alloy phase as Cu content increased. XPS results revealed that PtCu NPs had Pt enriched shells.

PtFe/GA was successfully synthesized via simultaneous SCD (Zhou et al., 2017). XRD data showed PtFe/GA had FCC structure with all plane angles shifted to higher 2θ values indicative of alloy formation. Furthermore, there was a shift of 0.3 eV in the Pt $4f_{5/2}$ peak in the Pt 4f XPS spectra for PtFe/GA compared to Pt/GA. TEM images showed that PtFe NPs were finely dispersed on GA with average NP 2.0 nm.

Recently, PtCu/CA was prepared via sequential SCD using $scCO_2$ followed by annealing (Barim et al., 2018). The effects of deposition order (either Pt or Cu first), Pt/Cu ratios, and annealing temperature on physical properties of the composite NPs were studied. Dimethyl(1,5-cyclooctadiene)platinum(II) and copper(II) trifluoroacetylacetonate precursors were adsorbed sequentially on the surface of CAs in presence of $scCO_2$ at 35°C and 10.7 MPa. In order to obtain the desired metal loading and composition, single metal adsorption isotherms for the MP-CA systems in $scCO_2$ were used. PtCu/CAs were annealed at different temperatures. XRD and TEM EDXS analyses showed that disordered PtCu alloy NPs were dispersed homogenously on the interior surface of CA. Alloyed fraction of total PtCu increased with increasing annealing temperature. Average PtCu alloy NP size increased from 1.8 to 4.5 nm with increasing annealing temperature.

SCD is an easily operated technique and has great potential to synthesize highly dispersed bimetallic NPs on aerogel supports without pH control of the solution. However, there are some disadvantages of this route. SCD requires SCF-soluble MPs which are more expensive compared to water-soluble counterparts. Low solubilities of some of the MPs in $scCO_2$ may lead to very long deposition times. The type of ligand and oxidation state of the metal of MPs were found to affect the solubility of the MPs in $scCO_2$ (Aschenbrenner et al., 2007). For complexes with the same ligand, as oxidation state of the metal atom increases, the MP becomes more soluble. Using ligands with higher solubility, such as fluorinated ligands or addition of a modifier may be beneficial to increase solubility of the precursors (Murphy and Erkey, 1997; Aggarwal et al., 2013).

Microwave-Assisted Deposition

Microwave assisted preparation of supported bimetallic NPs consists of preparation of a solution of the MP followed by the addition of the support to this solution. Subsequently, the solution is placed and heated in a microwave oven for a certain time at a desired microwave power and at practical microwave frequencies between 2.45 GHz and 900 MHz. Materials are then cooled down to room temperature, filtered, washed with deionized water and dried. Microwave technique enables the heating of materials or the reagent which possess adequate ratios of dielectric loss factor to dielectric constant via absorption of the microwave energy through molecular interaction with the electromagnetic field and then conversion to heat. During this process, MPs adsorb and convert to metal NPs on the support materials and the ligands should either desorb or be extracted with the washing step (Horikoshi and Serpone, 2016). PtCo/SA was prepared using the sequential approach where Co was first deposited using copper(II) nitrate via wet impregnation and $NaBH_4$ as the reducing agent which was followed by the deposition of Pt via microwave assisted route using hexachloroplatinic acid in ethylene glycol (Yu et al., 2016). Catalysts had good dispersion and 3 nm of average NP size according to TEM data.

PtAu/CA was prepared by simultaneous deposition of hexachloroplatinic acid and gold(III) chloride into CAs via microwave-assisted polyol route (Zhu et al., 2012). The sample was dried in vacuum oven at 80°C for 12 h. N_2 physisorption analysis indicated that CA had high surface area (637 m^2/g) and was mesoporous with an average pore diameter of 18.8 nm. XRD data showed shifts to lower 2θ degrees in all plane angles when compared to pure Pt. These shifts signify alloy formation between Pt and Au since lattice parameter of Au is higher than that of Pt. HRTEM images showed dispersed PtAu NPs on CA with little agglomeration and the average particle size was determined as 4.3 nm. Microwave assisted technique offers a relatively fast route for the preparation of supported bimetallic NPs. However, care must be taken to avoid hot spots that may form during microwave treatment that could potentially cause the agglomeration of NPs at certain regions of the support material.

Electroplating

Electroplating (electrodeposition) is usually performed to coat relatively flat surfaces with metal films for decorative purposes or to avoid metal corrosion. Technique is carried out in an electrolytic cell where a negative charge is applied on a support to be coated which is dipped to a solution containing positively charged metal cations which are then deposited onto the support due to applied potential difference (Rao and Trivedi, 2005). The electroplating approach was used to prepare FeCoP/GA (Zheng et al., 2016). Iron(II) sulfate, cobalt(II) sulfate, trisodium citrate, boric acid, sodium hypophosphite were dissolved in deionized water. The pH of the solution was adjusted to 5-6 using H_2SO_4. The temperature of the electrolyte was increased to 60°C. A GA with a height of about 5-10 mm was mounted on a titanium plate, which was used as a working electrode operating at a voltage of 1.0 V with respect to SCE. The samples were electroplated for 2-8 h. The resulting aerogel supported bimetallic NPs were amorphous according to XRD data and their sizes which varied between 30 and 100 nm depended on the plating time.

The electroplating technique offers a simple and conventional route to prepare metal/support composites that could be good candidates as electrocatalysts. However, the fact that the technique requires an electrode for the preparation of supported

NPs makes it difficult to decorate the inorganic supports used in non-electrocatalytic applications with NPs.

APPLICATIONS

Catalysis

Fuel cells are devices that convert chemical energy of a fuel, such as hydrogen and methanol into electricity by employing redox couple reactions occurring on an electrocatalyst surface. Since they are not heat engines, they are not bound by the Carnot cycle efficiency which makes them highly promising energy converters. Electrolyzers, on the other hand, utilizes electricity to convert water to hydrogen and oxygen on an electrocatalyst surface. Electrolyzers produce extremely pure hydrogen without any harmful emission making them suitable for use with hydrogen fuel cells to obtain a sustainable energy cycle (Zhang et al., 2016). Moreover, the energy obtained from renewable energy resources, such as sun, wind, and hydrothermal, can be stored in the chemical bonds of hydrogen through electrolyzers. Currently, hydrogen is mostly obtained by steam reforming of methane resulting in carbon dioxide emissions. Although, fuel cell and electrolyzers are quite advantageous from an environmental standpoint, the problems of durability, stability, poisoning and high cost of the noble metal based electrocatalysts have hindered their widespread utilization. Furthermore, electrolyzer technology requires the development of electrocatalysts with lower overpotential toward overall water splitting in order to reduce the energy consumption (Walter et al., 2010). Therefore, many research efforts are directed to improve electrocatalysts.

CAs are promising materials as electrocatalyst support in various electrochemical applications, such as fuel cells and electrolyzers due to their high electrical conductivity (Pekala, 1989; Maldonado-Hódar et al., 2000; Smirnova et al., 2005; Barim et al., 2017; Cai and Eychmüller, 2018). Recently, GA has emerged as a new class of electrically conductive, porous electrocatalyst support obtained via mild hydrothermal treatment of GO dispersions followed by supercritical or freeze-drying (Sarac Oztuna et al., 2017; Cai and Eychmüller, 2018). Importance of support material to obtain high performance electrocatalyst cannot be overstated since support significantly affects the parameters that are directly related to electrocatalytic activity, such as metal NP size and NP morphology. Supported metal NPs on CA, GA and their composites have been investigated for fuel cell and electrolyzer applications (Cai and Eychmüller, 2018).

The first study involving CA supported bimetallic NPs was conducted by utilizing PtRu/CA as electrocatalyst for DMFCs (Du et al., 2007). Results were compared with the commercial PtRu/C electrocatalyst. Commercial electrocatalyst showed the lowest onset potential toward methanol oxidation due to smaller PtRu NP size. Furthermore, increasing Ru content increased the onset potential and authors attributed it to the requirement of three neighboring Pt atoms for the adsorption and dehydrogenation of methanol which is the rate determining step in methanol oxidation. The maximum power density obtained from PtRu/CA and PtRu/C was similar although the metal content of PtRu/C was 1.5 times higher than that of PtCu/CA.

PtAu/CA was synthesized via microwave-assisted polyol method with the objective to improve the methanol tolerance of DMFC electrocatalysts (Zhu et al., 2012). High ratio of the oxidation current peak to reduction current peak (I_f/I_b) indicated a good methanol tolerance and PtAu/CA exhibited a higher I_f/I_b ratio than Pt/CA demonstrating the better performance of bimetallic systems. The authors also attributed this to the highly graphitized and mesoporous structure of CA that enhanced the electrical conductivity and mass transport, however, comparison to conventional supports, such as carbon blacks were not given.

The electrocatalytic activity of PtNi/CA was also investigated (Wang et al., 2017b) after theoretical calculations that indicated that $PtNi_3$ system gave the highest electrocatalytic performance toward ORR (Greeley and Nørskov, 2005). Prepared electrocatalyst showed 1.4 times higher mass activity at 0.9 V (vs. reversible hydrogen electrode, RHE) than commercial Pt/C. Furthermore, after accelerated stress tests, PtNi/CA electrocatalyst showed a 29% decrease in mass activity (35.7-25.3 mA/mgPt) whereas commercial Pt/C electrocatalyst exhibited a 52% decrease (25.2-12.1 mA/mgPt) indicating that highly porous structure of CA combined with the PtNi NPs resulted in highly durable and active ORR electrocatalysts. The methanol oxidation performance was also investigated in methanol added 0.5 M $HClO_4$ electrolyte. PtNi/CA gave slightly higher overpotential in the presence of methanol when compared to pure electrolyte, however, methanol tolerance was found to be higher than Pt/C.

PtFe/GA was synthesized and compared with Pt/GA (Zhou et al., 2017). Electrocatalysts were dealloyed electrochemically through continuous cycling to leach out Fe. New active sites were created with dealloying which was evident from the higher electrohemical surface area (ESA) of PtFe/GA (78 m^2/g) than commercial Pt/C (69 m^2/g). ORR curves of the dealloyed electrocatalyst shifted to higher potential when compared to commercial Pt/C. Furthermore, mass and specific activity of the dealloyed PtFe/GA were much higher than commercial Pt/C and also higher than the target set by U.S. Department of Energy, showing that highly active ORR electrocatalysts could be prepared by dealloying. Authors also compared Pt/GA and commercial Pt/C to investigate the effect of GA. Pt/GA showed 19 mV shift in the ORR curves to higher potential indicating that highly porous structure of GA resulted in maximized electrocatalyst surface area and enhanced mass transfer. The high activity of PtFe/GA can be attributed to the synergistic effects of GA support and alloying.

PtCu/CA also showed improved electrocatalytic activity toward ORR (Koh et al., 2008); therefore, ORR performance of PtCu/CA prepared via sequential SCD was investigated (Barim et al., 2018). Prior to electrochemical activity tests, electrocatalysts were dealloyed by continuous cycling in which ORR inactive excess Cu was selectively leached out of the PtCu NPs (Koh and Strasser, 2007; Dutta et al., 2010). Deposition order significantly affected the electrochemical performance as first Cu deposited samples showed no activity toward ORR due to Cu-enrichment on the surface of the PtCu alloy NPs

upon dealloying which resulted in unfavorable NP morphology. Optimum annealing temperature was determined as 800°C. Furthermore, electrocatalytic activity increased with increasing Pt:Cu mole ratio from 1:1 to 1:3 consistent with the earlier reports on similar systems (Koh et al., 2008). Electrocatalytic activities of the PtCu/CA samples were also compared with commercial Pt/C and higher ESA and mass activity (at 0.85 V vs. normal hydrogen electrode, NHE) were obtained with the dealloyed PtCu/CA prepared with a Pt:Cu mole ratio of 1:3 and annealed at 800°C (Barim et al., 2018).

For PEM fuel cells, electrode fabrication process involves applying an ink solution prepared by sonicating a solution of electrocatalyst and a binder to the surface of the carbon paper or the membrane. Subsequently, the membrane is sandwiched between two layers of carbon paper using a hot press to form a membrane electrode assembly (MEA). Utilizing binders may block the active sites and processes, such as sonication and hot pressing can destroy the structure of the electrocatalyst both of which lead to a decrease in electrocatalytic activity. PdPt/GA on NF was used as binder free anodes for direct glucose fuel cells (DGFCs) and direct ethanol fuel cells (DEFCs) (Tsang and Leung, 2017, 2018; Tsang et al., 2017, 2019). Authors suggested that the preparation of the electrocatalyst directly on the conductive and macroporous NF might eliminate the aforementioned problems. Fuel cell testing was also done using DGFC (batch) and DEFC (continuous) where PtPd/GA/NF was employed in the anode and Pt/C was employed in the cathode and results were compared with the monometallic counterparts. At a Pd:Pt ratio close to 1:1, PtPd/GA/NF exhibited higher maximum power density than the monometallic Pt/GA/NF and Pd/GA/NF for both reactions showing the synergistic effects of Pt and Pd leading to higher electrochemical performance. Binder (Nafion®) added PdPt/GA/NF electrode was also tested and resulted in a significantly lower maximum power density than that of binder-free electrode in both cases confirming the blockage of active sites via addition of binder. Supported Pd electrocatalysts also suffered from rapid degradation and poisoning (Li et al., 2016). N and S doped PdNi/CA NPs confined in carbon nanotubes (CNT) were tested for ethylene glycol oxidation by cyclic voltammetry (CV) in alkaline electrolyte and in a microfluidic direct ethylene glycol fuel cell (Raj kumar et al., 2019). Authors reported that CNT growth increased the flexibility of CA and the carbon shell around the PdNi NPs prevented agglomeration, delamination, and dissolution, hence increasing the stability. Prepared electrocatalyst exhibited superior electrochemical performance toward ethylene glycol oxidation than the monometallic Pd/CA and also Pt/C. Authors attributed the superior performance of PdNi/NSCNT/CA to the combined effects of PtNi and porous structure of CA that facilitated maximum utilization of fuel, enhanced the mass transport of fuel and ions and prevented the fuel crossover.

Non-PGM bimetallic systems were also investigated as electrocatalysts. The electrochemical activity of NiCo/MWCNTA (MWCNT aerogel supported NiCo) toward urea oxidation reaction was studied (Tesfaye et al., 2019). NiCo/MWCNTA showed a 50 mV decrease in onset potential for urea oxidation when compared to Ni/MWCNTA which was attributed to enhanced specific area and structural defects created with the addition of Co which evidently promoted the electron transfer by allowing Ni to reach a higher oxidation state. Authors also compared the performance of MWCNTA to conventional MWCNT powder and MWCNTA showed significantly lower onset potential indicating that high surface area and hierarchical pore structure of MWCNTA enhanced the mass transport which enhanced the electrochemical performance.

Recently, aerogel supported bimetallic NPs were also investigated as electrocatalysts for electrolyzers (Gu et al., 2018; Zhang et al., 2018). Currently used electrocatalysts are active for either oxygen evolution reaction (OER) or hydrogen evolution reaction (HER) and thus research efforts are directed to develop highly active and inexpensive bifunctional electrocatalysts for overall water splitting (Wang et al., 2017a; Zhang et al., 2017; Pan et al., 2018). CoFe/GAs which were N, S- and N-doped under different annealing conditions (N_2 or NH_3) were synthesized (Zhang et al., 2018). SEM images showed that the porous structure of rGO aerogel allowed high dispersion of CoFe NPs on the rGO sheets. Confinement within the graphene sheets prevented the dissolution and agglomeration of NPs by increasing the interfacial contact. Based on TEM and SEM images authors concluded that the annealing gas had no effect on the average CoFe NP size and the composition. However, it affected the morphology and the electrocatalytic activity of the resultant CoFe NPs. Annealing under N_2 atmosphere led to highly crystalline N, S-doped NPs $CoFe_2O_4$/GA which had low onset potential for OER whereas annealing under NH_3 led to amorphous N doped CoFe/GA NPs which had low onset potential for HER. N-doped NiFe/GA NPs with Ni:Fe mole ratio of 3:1 annealed under NH_3 environment were investigated for OER and HER (Gu et al., 2018). Prepared electrocatalyst showed high electrochemical activity toward OER and HER with good stability over 100 h in alkaline media. DFT calculations revealed the combined effects of Ni, Fe, and N enhanced the electrical conductivity and promoted electron transfer from metal NPs to rGO which in turn increased the activity and tuned the electronic distribution of metal nitrides on the surface.

There are numerous catalytic applications of aerogel supported bimetallic NPs other than electrochemistry. CO_2 reforming of methane for hydrogen production has been investigated due to the demand for safer, cleaner, and more economical energy sources. Reforming of methane can be done by dry methane reforming, steam methane reforming and methane oxidative CO_2 (Oxy-CO_2) reforming (Jang et al., 2019). Ni-based and Co-based catalysts are preferred over their noble metal counterparts for reforming reactions due to their lower price and wide availability, yet they suffer greatly from catalyst deactivation as a result of either coke formation or sintering of active metals. Nevertheless, CoNi bimetallic catalysts on various supports have been shown to yield higher or similar activities and longer stability for methane reforming compared to their monometallic counterparts (Takanabe et al., 2005; Koh et al., 2007; Chen et al., 2010), indicating that there is a synergistic effect between Co and Ni. Catalytic activity and stability of CoNi/AA catalysts, with 20% metal loading and Co:Ni ratio of 9, were investigated for methane oxy-CO_2 reforming (Chen et al.,

2010, 2011a, 2014). CoNi/AA performed better than Co/AA at various reactant gas ratios in a fixed bed reactor (Chen et al., 2010). XRD analysis on spent Co/AA showed that Co oxidized to less active Co_3O_4 during the reaction. XRD of fresh and spent CoNi/AA indicated the formation of CoNi metal alloy, and prevention of Co oxidation by the presence of Ni. Formation of metal alloy prevented metal sintering during reaction, which was also supported by H_2-TPR of calcined CoNi/AA. Suppression of Co oxidation and prevention of agglomerate formation by CoNi/AA was claimed to create a synergistic effect toward methane oxy-CO_2 reforming activity. In the same study, fixed bed reactor, conventional fluidized bed reactor, and magnetic assisted fluidized bed reactor (MAFB) were compared for methane oxy-CO_2 reforming activity of CoNi/AA catalyst. Due to enhanced gas-solid contact efficiency and longer residence time within the bed, MAFB was found to be the best performing reactor for this reaction. Among different ratios of Co:Ni of CoNi/AA catalyst (Co_xNi_y/AA, x and y being indicators of metal loading of Co and Ni, respectively where x, y = 0, 3, 5, 7, 10 wt% and x + y = 10), Co_5Ni_5/AA and Co_3Ni_7/AA were found to be the best performing catalysts in a fixed bed reactor (Chen et al., 2011a). TEM images showed that Co_5Ni_5/AA and Co_3Ni_7/AA catalysts had the smallest NP sizes after reduction. Since methane reforming is a structure sensitive reaction where defect sites, edges and kinks of metal NPs can be the active sites, catalysts with smaller particle sizes, where more metal-support interfacial structures occur, can result in higher activities. Afterwards, carbon deposition behavior was studied with different types of reactors. Again, MAFB was found to be the most suitable for methane oxy-CO_2 reforming reaction as the least catalyst deactivation occurred in this reactor (Chen et al., 2014).

Supercritical water gasification (SCWG) of biomass is an emerging technology for hydrogen production. In this process, biomass is hydrothermally converted to gaseous products at conditions above the critical point of water. Conventionally, SCWG is conducted using activated carbon, ZrO_2, Ru, Ni, NaOH, K_2CO_3, KOH, and Na_2CO_3 catalysts (Susanti et al., 2014). Among these, Ni-based catalysts are favorable because of their low price and availability; however, they suffer from coke deposition at high temperature applications. Addition of a noble metal as promoter has been shown to increase activity and selectivity toward hydrogen and decrease coke deposition (Mukainakano et al., 2007). Ru is known to prevent coke deposition and yield high activity and selectivity for SCWG. Therefore, Ru was incorporated as the promoter of Ni-based catalyst for SCWG of glucose (Hossain et al., 2017). Several RuNi/AA were compared with Ni/AA, Ni/Al_2O_3, and RuNi/Al_2O_3 xerogel (RuNi/AX) in terms of catalytic activity toward SCWG of glucose. H_2-TPR results showed that RuNi/AA had stronger metal-support interaction than RuNi/AX due to the presence of NiRu alloy. RuNi/AA gave the highest activity in tests carried out in a batch reactor. Spent catalysts were analyzed by XRD for deposited coke. Graphitic carbon peak was not observed in RuNi/AA and RuNi/AX after SCWG at 500°C. Formation of RuNi alloy, having strong metal-support interaction and high dispersion resulted in higher activity, selectivity, and effective prevention of coke deposition by RuNi/AA for SCWG of glucose.

Another route for hydrogen production is dehydrogenation of chemical hydrates. Ammonia borane (AB) is a suitable candidate for hydrogen production due to its high hydrogen content, stability, and solubility in water at room temperature. Noble metals, such as Pt, Ru, and Pd as well as non-noble metals, such as Co, Ni, Cu, and also their bimetallic combinations have been used for dehydrogenation of aqueous ammonia borane. In general, bimetallic catalysts were shown to exhibit higher H_2 yield. Aerogel supported Co-based catalysts were also shown to be catalytically more active than Co/MCM-41 due to higher dispersion of metals on aerogel support (Yu et al., 2015). To investigate the synergy between Co and Pt, PtCo/SA was compared with monometallic Pt/SA and Co/SA in terms of physical properties, activity, and stability (Yu et al., 2016). Six different bimetallic catalysts were prepared by varying the molar ratio of Pt:Co while keeping the loading amount of Co constant. Among bimetallic catalysts, the shortest time for complete hydrolysis was obtained with PtCo/SA having molar ratio of Pt:Co = 0.27:0.73, and which had highly dispersed small NPs without agglomeration. Reaction rates were found to be in the following order: Co/SA < Pt/SA < PtCo/SA. Turnover frequency of PtCo/SA was found to be 123.1 mol H_2/min. mol metal, which was higher than several previously reported multimetallic catalysts (Yu et al., 2016). This result was attributed to the synergy between closely contacted Pt and Co and/or formation of PtCo alloys.

Production of fine chemicals, polymers, perfumes, agrochemicals, and pharmaceuticals involves selective catalytic hydrogenation of unsaturated aldehydes. Selective cinnamaldehyde (CAL) hydrogenation to yield cinnamyl alcohol (COL) is facilitated by Pt-based catalysts. Some studies showed that introduction of a second metal may increase selectivity toward COL production (Vu et al., 2006; Guo et al., 2010). Pt/SA and PtCu/SA were synthesized and their activity toward selective hydrogenation of CAL were compared (Wang and Zhu, 2018). TOF of Pt/SA for COL production increased 10-fold when Cu was added. This increase was attributed to the increased fraction of Pt^0 on the surface of PtCu/SA due to increased electron transfer between Pt and Cu.

It is known that addition of transition metals, such as Co, Ni, and Cr or base metals, such as Na and K greatly enhances the activity of Pt toward oxidation reactions (Liu et al., 2012). The activities of Pt/SA and PtCo/SA toward CO preferential oxidation were compared with commercial Pt/Al_2O_3 (Choi et al., 2008). Pt/SA was prepared by solvent exchange of wet gels with ethanol solution of hexachloroplatinic acid. Cobalt(II) nitrate was added either in series by the same method (PtCo/SA), or by impregnation (Co/Pt/SA). Activity tests were conducted within a temperature range of 25-300°C. Overall, catalytic activities were in the order of Co/Pt/SA ≈ PtCo/SA >> Pt/SA > commercial Pt/Al_2O_3. Light-off temperature for bimetallic catalysts were around 70°C while it was around 170°C for Pt/SA and commercial Pt/Al_2O_3.

Fischer-Tropsch (FT) synthesis can be used for the production of transportation fuels from H_2 and CO obtained from renewable sources. The reaction yields paraffins, olefins, and alcohols; ranging from C_1 to C_{40} hydrocarbons (Mahmoudi et al., 2018).

Mostly used metal catalysts include Fe, Co, Ru, and Ni. Bimetallic FeCo catalysts, either in oxide form or as a FeCo alloy, were shown to improve product quality and selectivity, compared to monometallic analogs (Duvenhage and Coville, 2005). 5 and 10 wt% FeCo/SA were prepared for FT reaction (Loche et al., 2012). FeCo alloy formation was observed by X-ray absorption spectroscopy (XAS) after reduction with H_2 at 800°C. FeCo/SA became catalytically active after alloy formation and it yielded more than 20% CO conversion at 180°C. In general, 5 wt% catalyst showed lower conversion than 10 wt% catalyst while both were stable during runs which lasted from 72 to 96 h. Although different supports or monometallic counterparts of these catalysts were not studied in this research, comparison with literature (Bali et al., 2009) revealed that alloy FeCo/SA was active at lower temperatures compared to Fe aerogels and Fe xerogels; and did not need a promoter, such as potassium.

MWCNTs can be produced by catalytic chemical vapor deposition (CCVD) where hydrocarbons or alcohol gases are catalytically decomposed on a supported metal NPs to form CNTs. FeMo/SA was investigated for MWCNT production via CCVD (Marras et al., 2015). Three FeMo/SA catalysts were prepared with Fe:Mo weight ratio being 5:1, 3:1, or 0.7:1. All three catalyst were found to be effective for MWCNT production. The highest CNT yield was obtained at 800°C.

Optics

Noble metal bimetallic NPs, such as AgAu and AgCu exhibit enhanced surface plasmon resonance (SPR) with visible light at well-defined frequencies and when hosted in a dielectric matrix, they can give rise to enhanced optical effects in SERS which makes them ideal substrates in detection of chemical and biological species (Ferrando et al., 2008; Bigall et al., 2009; Chen et al., 2011b; Cortie and McDonagh, 2011; Fan et al., 2013; López Lozano et al., 2013; Tang et al., 2014; Wen and Eychmüller, 2017). The incident light interacts with the structural units of the aerogels in sub-optical wavelengths and generates intense local electromagnetic field at the so-called "hotspots" between NPs leading to signal enhancement. The recent studies revealed great potential of bimetallic aerogels for use as highly sensitive SERS platforms to detect environmental and biological target molecules of trace concentrations (Bigall et al., 2009; Wen and Eychmüller, 2017). The use of AuAg NPs in sensing platforms is gaining considerable attention due to their high extinction coefficients and unique size dependent optical properties (Liu et al., 2011; Patra and Gopinath, 2016). AuAg alloy NPs and self-supported AuAg bimetallic alloy aerogel monoliths were tested for SERS performance (Gao et al., 2016). The nanocomposites exhibited a remarkable sensing capability down to 1 nM with enhanced signal intensities that were 42 times than those obtained from the AuAg alloy NPs. The improvement in the SERS performance of the aerogels is attributed to their highly porous mesoporous three-dimensional structures with irregularities and surface roughness at the nanoscale, which can possibly form large number of hot spots. Unique features of aerogel structures were found to enhance the SERS signals (Sadrieyeh and Malekfar, 2018a). AgAu/TA nanocomposites with spherical NPs having estimated average size lower than 10 nm were used as the SERS substrates for the detection of a probe molecule, crystal violate. The highly porous nanocomposite networks enabled the probe to diffuse into the aerogel network with efficient interaction with the metal NPs, which resulted in detection of crystal violate in concentrations as low as 10^{-10} M.

Aerogels comprising of SPR-active NPs have been also gaining increasing attention to fabricate plasmonic photocatalysts with excellent light absorption and superior photocatalytic performances in various environmental and energy conversion applications. These materials are composed typically of noble-metal NPs and semiconductor photocatalysts supported in an aerogel matrix, which enable to spatially separate and electrochemically connect plasmonic sensitizers to metal NP co-catalyst (Rosseler et al., 2010; DeSario et al., 2017; Sadrieyeh and Malekfar, 2018a,b). Visible-light absorption is enhanced in these aerogel-based plasmonic photocatalysts through SPR and generates reactive electron-hole pairs to drive visible-light photochemistry and solar fuels chemistry (Rosseler et al., 2010; Lou et al., 2014; Patra and Gopinath, 2016; DeSario et al., 2017). AuAg/TA with enhanced photocatalytic activities were developed (Sadrieyeh and Malekfar, 2018b). Working principle of the photocatalyst AuAg/TA was illustrated in **Figure 5A**. The photocatalytic activities of the AgAu/TA were investigated through the degradation rate of a model compound, salicylic acid, under a solar simulator. It was demonstrated that photocatalytic activities of the nanocomposites were higher than pure TA regardless of the NP type, size and even the synthesis method (**Figure 5B**). TEM and FESEM images in **Figure 5C** along with nitrogen sorption experiments showed that the NPs were spherical with an average particle size between 6.5 and 7.5 nm, and they were embedded into interconnected porous network of TA. The metallic NPs enabled the absorption of longer wavelengths of solar spectra toward the visible.

The approach of coupling plasmonic metallic nanostructures in the porous network has the potential to impact a number of optical technologies including but not limited to solar energy harvesting, and photocatalysis. Owing to their unique physical and chemical properties including high electrical conductivity with effective surface area and mechanical strength, CAs have been particularly attractive in optoelectronic device applications, such as perovskite solar cells. A recent study demonstrated that core-shell hierarchical structured CoNi/CA with uniformly dispersed CoNi alloy particles with a particle diameter of 10-20 nm in the porous carbon medium could be successfully integrated in the solar cell assembly between the carbon electrode and the perovskite layer, thereby effectively improving the interface quality between the perovskite layer and the electrode and hole transporting ability (Xie et al., 2019). The number of optical and photonic applications of aerogels is expected to increase in the coming years, as the relationship between the nanostructure of aerogels and their optical properties is better understood. In addition, increasing market availability of different aerogels makes these materials attractive for the development of nanophotonic devices and ultra-lightweight plasmonic biosensors applications on a commercial scale.

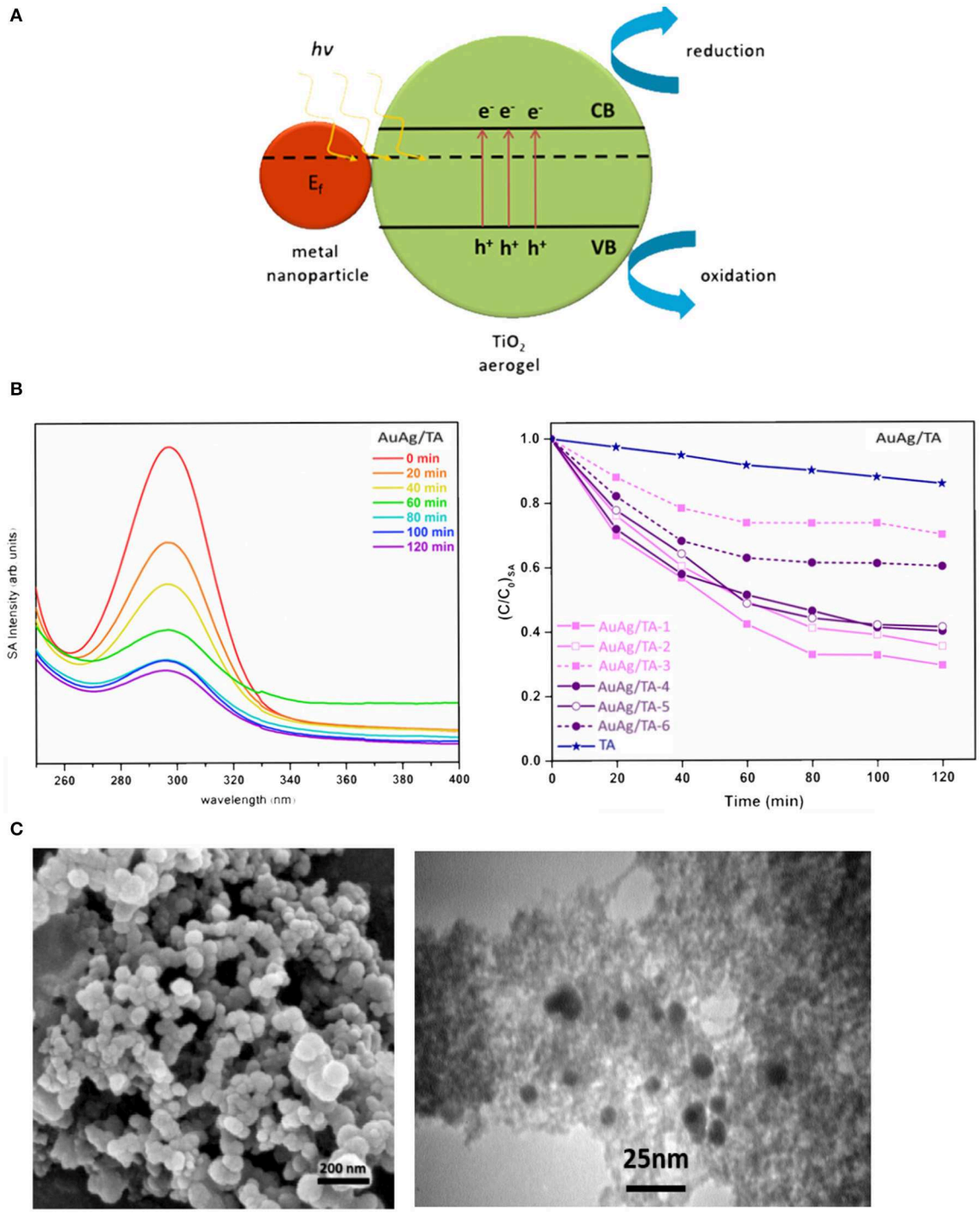

FIGURE 5 | (A) Schematic of plasmonic AuAg/TA, **(B)** photocatalytic performances of different AuAg/TA and pure TA, and **(C)** FESEM and TEM images of AuAg/TA. Reprinted from Sadrieyeh and Malekfar (2018b), ©2018, with permission from Elsevier.

Sensorics

Catalytic gas sensors are used for early leak detection of gases, such as hydrogen and hydrocarbons by a catalytic combustion reaction. Combustible gas sensors detect the temperature change caused by selective catalytic surface reaction between the target gas and oxidant. Aerogel supported metal nanocomposites can be used as the catalyst for this purpose. GA and boron nitride aerogel (BA) supported platinum or palladium NPs were used as the catalyst in a microheater-based combustible gas sensors (Harley-Trochimczyk et al., 2015). Hydrogen and propane

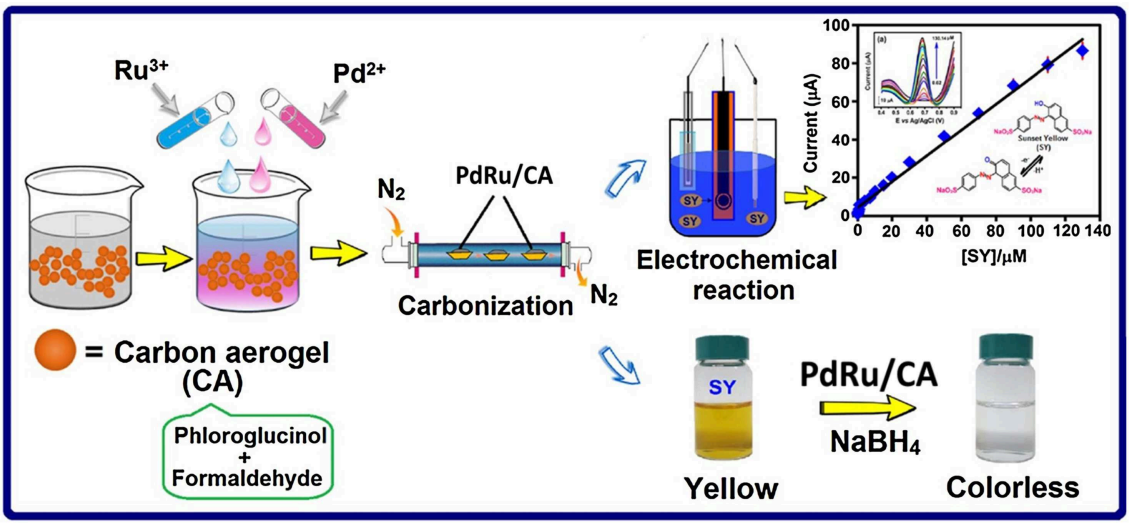

FIGURE 6 | Preparation and application of the PdRu/CA nanocomposite toward sensitive electrochemical detection of SY. Reprinted from Thirumalraj et al. (2018), ©2017, with permission from Elsevier.

could be detected with remarkable selectivity, faster response and recovery time when compared with commercial detectors (Harley-Trochimczyk et al., 2016). The promising performance of these type of sensors has attracted researchers' interests on the development of aerogel supported bimetallic catalysts toward sensing of chemical and biochemical materials.

Recently, PdRu/CA was studied as a catalyst for electrochemical detection of a food dye, sunset yellow (SY) (Thirumalraj et al., 2018). **Figure 6** summarizes the preparation of PdRu/CA catalyst via sol-gel route and usage of this catalyst in detection of SY. The electrochemical performances of the modified screen printed carbon electrode (SPCE) for detection of SY were evaluated by CV in $[Fe(CN)_6]^{3-/4-}$ electrolyte system. PdRu/CA-modified SPCE exhibited a more intense oxidation peak current and smaller peak to peak separation value, ΔE_p, indicating a higher conductivity and increased electrocatalytic activity of the electrode compared to other modified electrodes, especially Pd/CA catalyst. Furthermore, various concentrations of SY (0.02-130.14 μM) were correlated with intensity of oxidation peak current by a linear equation. Incorporation of Ru as the secondary metal provided synergy between bimetallic PdRu NPs and the porous CA support which improved the electron transfer process during electrooxidation of SY. There are very few studies on aerogel supported bimetallic sensors, however they have a great potential for detection of chemical and biochemical compounds.

CONCLUSIONS AND FUTURE DIRECTIONS

The aerogel market is growing at an accelerated pace and is expected to reach 1.27 billion USD in 2026[1]. The market price of a wide variety of aerogels is also decreasing due to the advancements in aerogel production technologies. For example, improvements in our understanding of the supercritical drying process is leading to reductions in operating pressures and drying times which are reducing the capital and operational costs of aerogel production (Özbakir and Erkey, 2015; Sahin et al., 2017, 2019). Using aerogels instead of conventional porous materials as supports for bimetallic NPs is becoming more attractive due to their open and interconnected pore structure, high porosity, high surface area and easily tunable properties. Therefore, aerogel supported bimetallic NPs can be considered as an emerging class of nanocomposites with superior properties with potential applications in optics, catalysis, adsorption, and medicine. Despite their potential, only a very small fraction of possible kinds and compositions of metallic NPs on aerogel supports have been synthesized and studied until now. Further studies on synthesis with different bimetallic NPs and different kinds of aerogels are definitely needed. There is a very limited number of studies which compare the performance of non-aerogel supported and aerogel supported bimetallic NPs. It is well known that support type can alter textural properties and performance of a nanocomposite as a result of different metal-support interactions, porosity of the support, thermal and chemical stability. Studies are needed on comparison of aerogel supported and non-aerogel supported bimetallic NPs in order to fully reveal the potential of combining superior properties of aerogels as support and bimetallic NPs.

Newer techniques, such as SCD and pulsed laser deposition have potential to produce materials that cannot be produced with conventional techniques. Understanding the factors controlling the morphology, size, and composition of these bimetallic NPs on the interior surface of aerogel supports is necessary so that these can be tuned to desired levels for a specific application. In the case of SCD, it is important to understand the adsorption kinetics of MPs in order to control NP size and metal loading

[1]https://www.prnewswire.com/news-releases/aerogel-market-to-reach-usd-2-97-billion-by-2026--reports-and-data-300943078.html

(Bozbag et al., 2013). Binary adsorption kinetics may differ from single component kinetics (Bozbag et al., 2011). Investigation of binary adsorption isotherms may be very beneficial for further development of preparation of aerogel supported bimetallic NPs via SCD.

Studies on the effects of the surface chemistry and morphology of the aerogels on the formation and growth of nanoalloy particles would be especially welcome. Along this line, coupling *in-situ* characterization studies with computational atomic scale modeling should be extremely beneficial and accelerate the development of these materials for commercial applications. Surface modification of aerogels can enhance their properties, such as surface charge, surface energy, roughness, hydrophilicity, reactivity, electronic, magnetic, and mechanical properties (Sanli and Erkey, 2015). Using surface-modified aerogels as supports for bimetallic NPs can enhance the performance and even broaden the application range of this emerging class of nanocomposites.

Although aerogels have been shown to be good support materials for catalysis and sensorics applications, it is important to note that they may suffer from pore collapse when the aerogel is contacted with a liquid phase, or when temperature and pressure changes result in condensation of vapor phase within the pores of aerogels or increased surface tension. This can be overcome by using aerogels having higher density. While denser aerogels have smaller porosity, their network strength is higher which may prevent pore collapse (Deshpande et al., 1992).

The newly developing electrochemical energy conversion systems, such as alkaline fuel cells, water, and CO_2 electrolyzers and lithium ion batteries will definitely benefit from the superior properties of CA or GA supported bimetallic NPs. SA supported bimetallic NPs with high transparency could also have potential applications in photovoltaics or in photoelectrochemical processes.

Combining the optical and electronic properties of bimetallic NPs supported on aerogels could lead to the development of smarter materials in a variety of areas ranging from electronics to textiles. The need for the versatility of textural properties such the combination of micro and mesostructured support materials is accelerating for many areas including industrial catalysis. Aerogel supported bimetallic NPs and their composites with microporous materials such the MOFs (Ulker et al., 2013; Inonu et al., 2018) could bring many advantages, such as selectivity control for such processes. No studies on using carbohydrate aerogels as supports for bimetallic NPs have been reported so far. Their cheap price and interesting properties should lead to development of exciting nanostructured materials for a wide variety of applications in sensing and medicine (Ganesan et al., 2018; Wang et al., 2019). Organic-inorganic hybrid aerogels have been gaining attention due to their enhanced thermal and mechanical properties (Pirzada et al., 2019). Combining unique characteristics of organic and inorganic aerogels, hybrid aerogels can be used in extended fields of application. They have already been used as superinsulators, electrodes, and absorbents to separate oil-water mixtures (Kanamori, 2016), they can also be used as support materials for NPs. There is a limited number of studies on aerogel supported trimetallic NPs. Incorporation of a third metal can further enhance the performance of the nanocomposites in electrocatalysis (Kolla and Smirnova, 2015; Zhou et al., 2017). This knowledge can be applied to other applications as well.

We expect that our review on aerogel supported bimetallic NPs will pave the way for both experimental and theoretical researchers to broaden the applications of these nanocomposites and to incorporate with novel technologies for the invention of nanocomposites with even more improved properties in the future.

AUTHOR CONTRIBUTIONS

All authors listed have made a substantial, direct and intellectual contribution to the work, and approved it for publication.

REFERENCES

Aggarwal, V., Reichenbach, L. F., Enders, M., Muller, T., Wolff, S., Crone, M., et al. (2013). Influence of perfluorinated end groups on the SFRD of [Pt(cod)Me(C_nF_{2n+1})] onto porous Al_2O_3 in CO_2 under reductive conditions. *Chem. A Eur. J.* 19, 12794-12799. doi: 10.1002/chem.201301191

Antolini, E. (2009). Carbon supports for low-temperature fuel cell catalysts. *Appl. Catal. B Environ.* 88, 1-24. doi: 10.1016/j.apcatb.2008.09.030

Aschenbrenner, O., Kemper, S., Dahmen, N., Schaber, K., and Dinjus, E. (2007). Solubility of B-diketonates, cyclopentadienyls, and cyclooctadiene complexes with various metals in supercritical carbon dioxide. *J. Supercrit. Fluids* 41, 179–186. doi: 10.1016/j.supflu.2006.10.011

Bali, S., Huggins, F. E., Huffman, G. P., Ernst, R. D., Pugmire, R. J., and Eyring, E. M. (2009). Iron aerogel and xerogel catalysts for Fischer–Tropsch synthesis of diesel fuel. *Energy Fuels* 23, 14–18. doi: 10.1021/ef8005367

Barim, B., Bayrakçeken, A., Bozbag, S. E., Zhang, L., Kizilel, R., Aindow, M., et al. (2017). Control of average particle size of carbon aerogel supported platinum nanoparticles by supercritical deposition. *Microporous Mesoporous Mater.* 245, 94–103. doi: 10.1016/j.micromeso.2017.01.037

Barim, S. B., Bozbag, S. E., Yu, H., Kizilel, R., Aindow, M., and Erkey, C. (2018). Mesoporous carbon aerogel supported PtCu bimetallic nanoparticles via supercritical deposition and their dealloying and electrocatalytic behaviour. *Catal. Today* 310, 166–175. doi: 10.1016/j.cattod.2017.09.023

Bayrakçeken, A., Cangül, B., Zhang, L. C., Aindow, M., and Erkey, C. (2010). PtPd/BP2000 electrocatalysts prepared by sequential supercritical carbon dioxide deposition. *Int. J. Hydrogen Energy* 35, 11669–11680. doi: 10.1016/j.ijhydene.2010.08.059

Bigall, N. C., Herrmann, A. K., Vogel, M., Rose, M., Simon, P., Carrillo-Cabrera, W., et al. (2009). Hydrogels and aerogels from noble metal nanoparticles. *Angew. Chem. Int. Ed.* 48, 9731–9734. doi: 10.1002/anie.200902543

Bosco, J. P., Humbert, M. P., and Chen, J. G. (2009). "Design of bimetallic catalysts: from model surfaces to supported catalysts," in *Design of Heterogeneous Catalysts: New Approaches Based on Synthesis, Characterization and Modeling*, ed U. S. Ozkan (Weinheim: Wiley-VCH Verlag GmbH & Co. KGaA), 195–212. doi: 10.1002/9783527625321.ch8

Bourikas, K., Kordulis, C., and Lycourghiotis, A. (2006). The role of the liquid-solid interface in the preparation of supported catalysts. *Catal. Rev.* 48, 363–444. doi: 10.1080/01614940600962321

Bozbag, S. E., and Erkey, C. (2015). Supercritical deposition: Current status and perspectives for the preparation of supported metal nanostructures. *J. Supercrit. Fluids* 96, 298–312. doi: 10.1016/j.supflu.2014.09.036

Bozbag, S. E., Sanli, D., and Erkey, C. (2012). Synthesis of nanostructured materials using supercritical CO_2: part II. Chemical transformations. *J. Mater. Sci.* 47, 3469–3492. doi: 10.1007/s10853-011-6064-9

Bozbag, S. E., Unal, U., Kurykin, M. A., Ayala, C. J., Aindow, M., and Erkey, C. (2013). Thermodynamic control of metal loading and composition of carbon aerogel supported Pt–Cu alloy nanoparticles by supercritical deposition. *J. Phys. Chem. C* 117, 6777–6787. doi: 10.1021/jp311641g

Bozbag, S. E., Yasar, N. S., Zhang, L. C., Aindow, M., and Erkey, C. (2011). Adsorption of Pt(cod)me_2 onto organic aerogels from supercritical solutions for the synthesis of supported platinum nanoparticles. *J. Supercrit. Fluids* 56, 105–113. doi: 10.1016/j.supflu.2010.10.045

Cai, B., and Eychmüller, A. (2018). Promoting electrocatalysis upon aerogels. *Adv. Mater.* 31:e1804881. doi: 10.1002/adma.201804881

Cangül, B., Zhang, L. C., Aindow, M., and Erkey, C. (2009). Preparation of carbon black supported Pd, Pt and Pd–Pt nanoparticles using supercritical CO_2 deposition. *J. Supercrit. Fluids* 50, 82–90. doi: 10.1016/j.supflu.2009.04.001

Casu, A., Casula, M. F., Corrias, A., Falqui, A., Loche, D., Marras, S., et al. (2008). The influence of composition and porosity on the magnetic properties of FeCo-SiO_2 nanocomposite aerogels. *Phys. Chem. Chem. Phys.* 10, 1043–1052. doi: 10.1039/b712719g

Casula, M. F., Concas, G., Congiu, F., Corrias, A., Falqui, A., and Spano, G. (2005). Near equiatomic FeCo nanocrystalline alloy embedded in an alumina aerogel matrix: microstructural features and related magnetic properties. *J. Phys. Chem. B* 109, 23888–23895. doi: 10.1021/jp0546554

Casula, M. F., Corrias, A., and Paschina, G. (2002). FeCo-SiO_2 nanocomposite aerogels by high temperature supercritical drying. *J. Mater. Chem.* 12, 1505–1510. doi: 10.1039/b110093a

Casula, M. F., Corrias, A., and Paschina, G. (2003). Iron-Cobalt-Silica aerogel nanocomposite materials. *J. Sol Gel Sci. Technol.* 26, 667–670. doi: 10.1023/A:1020761130074

Casula, M. F., Loche, D., Marras, S., Paschina, G., and Corrias, A. (2007). Role of urea in the preparation of highly porous nanocomposite aerogels. *Langmuir* 23, 3509–3512. doi: 10.1021/la0635799

Chen, L., Hao, Z., Yang, T., Liu, W., and Zhang, D. (2014). Carbon deposition behavior of a Co-Ni aerogel catalyst in CH_4 oxy-CO_2 reforming using various types of reactors. *Int. J. Hydrog. Energy* 39, 15474–15481. doi: 10.1016/j.ijhydene.2014.07.128

Chen, L., Zhu, Q., Hao, Z., Zhang, T., and Xie, Z. (2010). Development of a Co–Ni bimetallic aerogel catalyst for hydrogen production via methane oxidative CO_2 reforming in a magnetic assisted fluidized bed. *Int. J. Hydrog. Energy* 35, 8494–8502. doi: 10.1016/j.ijhydene.2010.06.003

Chen, L., Zhu, Q., and Wu, R. (2011a). Effect of Co-Ni ratio on the activity and stability of Co-Ni bimetallic aerogel catalyst for methane Oxy-CO_2 reforming. *Int. J. Hydrog. Energy* 36, 2128–2136. doi: 10.1016/j.ijhydene.2010.11.042

Chen, Y., Ng, K. C., Yan, W., Tang, Y., and Cheng, W. (2011b). Ultraflexible plasmonic nanocomposite aerogel. *RSC Adv.* 1, 1265–1270. doi: 10.1039/c1ra00532d

Choi, J., Shin, C. B., and Suh, D. J. (2008). Co-promoted Pt catalysts supported on silica aerogel for preferential oxidation of CO. *Catal. Commun.* 9, 880–885. doi: 10.1016/j.catcom.2007.09.036

Corrias, A., and Casula, M. F. (2011). "Aerogels containing metal, alloy, and oxide nanoparticles embedded into dielectric matrices," in *Aerogels Handbook*, eds M. A. Aegerter, N. Leventis, and M. M. Koebel (New York, NY: Springer), 335–363. doi: 10.1007/978-1-4419-7589-8_16

Corrias, A., Casula, M. F., Falqui, A., and Paschina, G. (2004). Preparation and characterization of FeCo-Al_2O_3 and Al_2O_3 aerogels. *J. Sol-Gel Sci. Technol.* 31, 83–86. doi: 10.1023/B:JSST.0000047965.22232.53

Cortie, M. B., and McDonagh, A. M. (2011). Synthesis and optical properties of hybrid and alloy plasmonic nanoparticles. *Chem. Rev.* 111, 3713–3735. doi: 10.1021/cr1002529

Da Silva, R. O., Heiligtag, F. J., Karnahl, M., Junge, H., Niederberger, M., and Wohlrab, S. (2015). Design of multicomponent aerogels and their performance in photocatalytic hydrogen production. *Catal. Today* 246, 101–107. doi: 10.1016/j.cattod.2014.08.028

Deka, U., Lezcano-Gonzalez, I., Weckhuysen, B. M., and Beale, A. M. (2013). Local environment and nature of Cu active sites in zeolite-based catalysts for the selective catalytic reduction of NO_x. *ACS Catal.* 3, 413–427. doi: 10.1021/cs300794s

DeSario, P. A., Pietron, J. J., Dunkelberger, A., Brintlinger, T. H., Baturina, O., Stroud, R. M., et al. (2017). Plasmonic aerogels as a three-dimensional nanoscale platform for solar fuel photocatalysis. *Langmuir* 33, 9444–9454. doi: 10.1021/acs.langmuir.7b01117

Deshpande, R., Hua, D. W., Smith, D. M., and Brinker, C. J. (1992). Pore structure evolution in silica gel during aging/drying. III. Effects of surface tension. *J. Non Cryst. Solids* 144, 32–44. doi: 10.1016/S0022-3093(05)80380-1

Du, H., Li, B., Kang, F., Fu, R., and Zeng, Y. (2007). Carbon aerogel supported Pt–Ru catalysts for using as the anode of direct methanol fuel cells. *Carbon* 45, 429–435. doi: 10.1016/j.carbon.2006.08.023

Dutta, I., Carpenter, M. K., Balogh, M. P., Ziegelbauer, J. M., Moylan, T. E., Atwan, M. H., et al. (2010). Electrochemical and structural study of a chemically dealloyed PtCu oxygen reduction catalyst. *J. Phys. Chem. C* 114, 16309–16320. doi: 10.1021/jp106042z

Duvenhage, D. J., and Coville, N. J. (2005). Fe:Co/TiO_2 bimetallic catalysts for the Fischer-Tropsch reaction: part 3: the effect of Fe:Co ratio, mixing and loading on FT product selectivity. *Appl. Catal. A Gen.* 289, 231–239. doi: 10.1016/j.apcata.2005.05.008

Eppler, A. S., Rupprechter, G., Guczi, L., and Somorjai, G. A. (1997). Model catalysts fabricated using electron beam lithography and pulsed laser deposition. *J. Phys. Chem. B* 101, 9973–9977. doi: 10.1021/jp972818l

Erkey, C. (2009). Preparation of metallic supported nanoparticles and films using supercritical fluid deposition. *J. Supercrit. Fluids* 47, 517–522. doi: 10.1016/j.supflu.2008.10.019

Fan, M., Lai, F. J., Chou, H. L., Lu, W. T., Hwang, B. J., and Brolo, A. G. (2013). Surface-enhanced Raman scattering (SERS) from Au:Ag bimetallic nanoparticles: the effect of the molecular probe. *Chem. Sci.* 4, 509–515. doi: 10.1039/C2SC21191B

Ferrando, R., Jellinek, J., and Johnston, R. L. (2008). Nanoalloys: from theory to applications of alloy clusters and nanoparticles. *Chem. Rev.* 108, 845–910. doi: 10.1021/cr040090g

Ganesan, K., Budtova, T., Ratke, L., Gurikov, P., Baudron, V., Preibisch, I., et al. (2018). Review on the production of polysaccharide aerogel particles. *Materials* 11:2144. doi: 10.3390/ma11112144

Gao, X., Esteves, R. J. A., Nahar, L., Nowaczyk, J., and Arachchige, I. U. (2016). Direct cross-linking of Au/Ag alloy nanoparticles into monolithic aerogels for application in surface-enhanced raman scattering. *ACS Appl. Mater. Interfaces* 8, 13076–13085. doi: 10.1021/acsami.5b11582

Ghosh Chaudhuri, R., and Paria, S. (2012). Core/shell nanoparticles: classes, properties, synthesis mechanisms, characterization, and applications. *Chem. Rev.* 112, 2373–2433. doi: 10.1021/cr100449n

Gómez-Cápiro, O., Hinkle, A., Delgado, A. M., Fernández, C., Jiménez, R., and Arteaga-Pérez, L. E. (2018). Carbon aerogel-supported nickel and iron for gasification gas cleaning. Part I: ammonia adsorption. *Catalysts* 8:347. doi: 10.3390/catal8090347

Greeley, J., and Nørskov, J. K. (2005). A general scheme for the estimation of oxygen binding energies on binary transition metal surface alloys. *Surf. Sci.* 592, 104–111. doi: 10.1016/j.susc.2005.07.018

Gu, Y., Chen, S., Ren, J., Jia, Y. A., Chen, C., Komarneni, S., et al. (2018). Electronic structure tuning in Ni_3FeN/r-GO aerogel toward bifunctional electrocatalyst for overall water splitting. *ACS Nano* 12, 245–253. doi: 10.1021/acsnano.7b05971

Guo, Z., Chen, Y., Li, L., Wang, X., Haller, G. L., and Yang, Y. (2010). Carbon nanotube-supported Pt-based bimetallic catalysts prepared by a microwave-assisted polyol reduction method and their catalytic applications in the selective hydrogenation. *J. Catal.* 276, 314–326. doi: 10.1016/j.jcat.2010.09.021

Han, X., Wang, M., Le, M. L., Bedford, N. M., Woehl, T. J., and Thoi, V. S. (2019). Effects of substrate porosity in carbon aerogel supported copper for electrocatalytic carbon dioxide reduction. *Electrochim. Acta* 297, 545–552. doi: 10.1016/j.electacta.2018.11.203

Harley-Trochimczyk, A., Chang, J., Pham, T., Dong, J., Worsley, M. A., Zettl, A., et al. (2015). "Low power microheater-based combustible gas sensor with graphene aerogel catalyst support," in *2015 Transducers - 2015 18th International Conference on Solid-State Sensors, Actuators and Microsystems, TRANSDUCERS 2015* (Anchorage, AK: Institute of Electrical and Electronics Engineers Inc.), 1483–1486. doi: 10.1109/TRANSDUCERS.2015.7181216

Harley-Trochimczyk, A., Pham, T., Chang, J., Chen, E., Worsley, M. A., Zettl, A., et al. (2016). Platinum nanoparticle loading of boron nitride aerogel and its use

as a novel material for low-power catalytic gas sensing. *Adv. Funct. Mater.* 26, 433–439. doi: 10.1002/adfm.201503605

Hayase, G., Kugimiya, K., Ogawa, M., Kodera, Y., Kanamori, K., and Nakanishi, K. (2014). The thermal conductivity of polymethylsilsesquioxane aerogels and xerogels with varied pore sizes for practical application as thermal superinsulators. *J. Mater. Chem. A* 2, 6525–6531. doi: 10.1039/C3TA15094A

Heinrichs, B., Delhez, P., Schoebrechts, J. P., and Pirard, J. P. (1997). Palladium-silver sol-gel catalysts for selective hydrodechlorination of 1,2-dichloroethane into ethylene: I. Synthesis and characterization. *J. Catal.* 172, 322–335. doi: 10.1006/jcat.1997.1881

Herrmann, A. K., Formanek, P., Borchardt, L., Klose, M., Giebeler, L., Eckert, J., et al. (2014). Multimetallic aerogels by template-free self-assembly of Au, Ag, Pt, and Pd nanoparticles. *Chem. Mater.* 26, 1074–1083. doi: 10.1021/cm4033258

Horikoshi, S., and Serpone, N. (2016). "Preparation of heterogeneous catalysts by a microwave selective heating method," in *Microwaves in Catalysis: Methodology and Applications*, eds S. Horikoshi and N. Serpone (Weinheim: Wiley-VCH Verlag GmbH & Co.), 79–103. doi: 10.1002/9783527688111.ch5

Hossain, M. Z., Chowdhury, M. B. I., Jhawar, A. K., and Charpentier, P. A. (2017). Supercritical water gasification of glucose using bimetallic aerogel Ru-Ni-Al_2O_3 catalyst for H_2 production. *Biomass Bioenerg.* 107, 39–51. doi: 10.1016/j.biombioe.2017.09.010

Hund, J. F., Bertino, M. F., Zhang, G., Sotiriou-Leventis, C., and Leventis, N. (2004). Synthesis of homogeneous alloy metal nanoparticles in silica aerogels. *J. Non Cryst. Solids* 350, 9–13. doi: 10.1016/j.jnoncrysol.2004.06.037

Inonu, Z., Keskin, S., and Erkey, C. (2018). An emerging family of hybrid nanomaterials: metal–organic framework/aerogel composites. *ACS Appl. Nano Mater.* 1, 5959–5980. doi: 10.1021/acsanm.8b01428

Jang, W. J., Shim, J. O., Kim, H. M., Yoo, S. Y., and Roh, H. S. (2019). A review on dry reforming of methane in aspect of catalytic properties. *Catal. Today* 324, 15–26. doi: 10.1016/j.cattod.2018.07.032

Jin, Y., Zhao, G., Wu, M., Lei, Y., Li, M., and Jin, X. (2011). *In situ* induced visible-light photoeletrocatalytic activity from molecular oxygen on carbon aerogel-supported TiO_2. *J. Phys. Chem. C* 115, 9917–9925. doi: 10.1021/jp2009429

Job, N., Heinrichs, B., Ferauche, F., Noville, F., Marien, J., and Pirard, J. P. (2005). Hydrodechlorination of 1,2-dichloroethane on Pd-Ag catalysts supported on tailored texture carbon xerogels. *Catal. Today* 102, 234–241. doi: 10.1016/j.cattod.2005.02.021

Kanamori, K. (2016). "Hybrid aerogels," in *Handbook of Sol-Gel Science and Technology*, eds L. Klein, M. Aparicio, and A. Jitianu (Cham: Springer International Publishing), 1–22. doi: 10.1007/978-3-319-19454-7_89-1

Kanamori, K., Aizawa, M., Nakanishi, K., and Hanada, T. (2007). New transparent methylsilsesquioxane aerogels and xerogels with improved mechanical properties. *Adv. Mater.* 19, 1589. doi: 10.1002/adma.200602457

Kanamori, K., Aizawa, M., Nakanishi, K., and Hanada, T. (2008). Elastic organic-inorganic hybrid aerogels and xerogels. *J. Sol-Gel Sci. Technol.* 48, 172–181. doi: 10.1007/s10971-008-1756-6

Kistler, S. S. (1931). Coherent expanded aerogels and jellies. *Nature* 127:741. doi: 10.1038/127741a0

Kitchin, J. R., Nørskov, J. K., Barteau, M. A., and Chen, J. G. (2004). Role of strain and ligand effects in the modification of the electronic and chemical properties of bimetallic surfaces. *Phys. Rev. Lett.* 93:156801. doi: 10.1103/PhysRevLett.93.156801

Koh, A. C. W., Chen, L., Kee Leong, W., Johnson, B. F. G., Khimyak, T., and Lin, J. (2007). Hydrogen or synthesis gas production via the partial oxidation of methane over supported nickel-cobalt catalysts. *Int. J. Hydrogen Energy* 32, 725–730. doi: 10.1016/j.ijhydene.2006.08.002

Koh, S., Hahn, N., Yu, C., and Strasser, P. (2008). Effects of composition and annealing conditions on catalytic activities of dealloyed Pt-Cu nanoparticle electrocatalysts for PEMFC. *J. Electrochem. Soc.* 155, B1281–B1288. doi: 10.1149/1.2988741

Koh, S., and Strasser, P. (2007). Electrocatalysis on bimetallic surfaces: Modifying catalytic reactivity for oxygen reduction by voltammetric surface dealloying. *J. Am. Chem. Soc.* 129, 12624–12625. doi: 10.1021/ja0742784

Kolla, P., and Smirnova, A. (2015). Methanol oxidation and oxygen reduction activity of PtIrCo-alloy nanocatalysts supercritically deposited within 3D carbon aerogel matrix. *Electrochim. Acta*. 182, 20–30. doi: 10.1016/j.electacta.2015.09.033

Lambert, S., Ferauche, F., Brasseur, A., Pirard, J. P., and Heinrichs, B. (2005). Pd-Ag/SiO_2 and Pd-Cu/SiO_2 cogelled xerogel catalysts for selective hydrodechlorination of 1,2-dichloroethane into ethylene. *Catalysis Today* 100, 283–289. doi: 10.1016/j.cattod.2004.08.015

Li, L., He, S., Liu, M., Zhang, C., and Chen, W. (2015). Three-dimensional mesoporous graphene aerogel-supported SnO_2 nanocrystals for high-performance NO_2 gas sensing at low temperature. *Anal. Chem.* 87, 1638–1645. doi: 10.1021/ac503234e

Li, S., Lai, J., Luque, R., and Xu, G. (2016). Designed multimetallic Pd nanosponges with enhanced electrocatalytic activity for ethylene glycol and glycerol oxidation. *Energy Environ. Sci.* 9, 3097–3102. doi: 10.1039/C6EE02229D

Liu, K., Wang, A., and Zhang, T. (2012). Recent advances in preferential oxidation of co reaction over platinum group metal catalysts. *ACS Catal.* 2, 1165–1178. doi: 10.1021/cs200418w

Liu, S., Chen, G., Prasad, P. N., and Swihart, M. T. (2011). Synthesis of monodisperse Au, Ag, and Au-Ag alloy nanoparticles with tunable size and surface plasmon resonance frequency. *Chem. Mater.* 23, 4098–4101. doi: 10.1021/cm201343k

Liu, W., Herrmann, A. K., Bigall, N. C., Rodriguez, P., Wen, D., Oezaslan, M., et al. (2015). Noble metal aerogels-synthesis, characterization, and application as electrocatalysts. *Acc. Chem. Res.* 48, 154–162. doi: 10.1021/ar500237c

Liu, W., Rodriguez, P., Borchardt, L., Foelske, A., Yuan, J., Herrmann, A. K., et al. (2013). Bimetallic aerogels: High-performance electrocatalysts for the oxygen reduction reaction. *Angew. Chem. Int. Ed.* 52, 9849–9852. doi: 10.1002/anie.201303109

Liu, X., Cui, J., Sun, J., and Zhang, X. (2014). 3D graphene aerogel-supported SnO_2 nanoparticles for efficient detection of NO_2. *RSC Adv.* 4, 22601–22605. doi: 10.1039/c4ra02453b

Loche, D., Casula, M. F., Corrias, A., Marras, S., and Moggi, P. (2012). Bimetallic FeCo nanocrystals supported on highly porous silica aerogels as fischer-tropsch catalysts. *Catal. Lett.* 142, 1061–1066. doi: 10.1007/s10562-012-0877-2

López Lozano, X., Mottet, C., and Weissker, H. C. (2013). Effect of alloying on the optical properties of Ag-Au nanoparticles. *J. Phys. Chem. C* 117, 3062–3068. doi: 10.1021/jp309957y

Lou, Z., Wang, Z., Huang, B., and Dai, Y. (2014). Synthesis and activity of plasmonic photocatalysts. *ChemCatChem* 6, 2456–2476. doi: 10.1002/cctc.201402261

Mahmoudi, H., Mahmoudi, M., Doustdar, O., Jahangiri, H., Tsolakis, A., Gu, S., et al. (2018). A review of Fischer Tropsch synthesis process, mechanism, surface chemistry and catalyst formulation. *Biofuels Eng.* 2, 11–31. doi: 10.1515/energyo.0128.00001

Maldonado-Hódar, F. J., Moreno-Castilla, C., Rivera-Utrilla, J., Hanzawa, Y., and Yamada, Y. (2000). Catalytic graphitization of carbon aerogels by transition metals. *Langmuir* 16, 4367–4373. doi: 10.1021/la991080r

Mani, P., Srivastava, R., and Strasser, P. (2008). Dealloyed Pt-Cu core-shell nanoparticle electrocatalysts for use in PEM fuel cell cathodes. *J. Phys. Chem. C* 112, 2770–2778. doi: 10.1021/jp0776412

Marras, C., Loche, D., Corrias, A., Konya, Z., and Casula, M. F. (2015). Bimetallic Fe/Mo–SiO_2 aerogel catalysts for catalytic carbon vapour deposition production of carbon nanotubes. *J. Sol-Gel Sci. Technol.* 73, 379–388. doi: 10.1007/s10971-014-3544-9

Mehrabadi, B. A. T., Eskandari, S., Khan, U., White, R. D., and Regalbuto, J. R. (2017). "A review of preparation methods for supported metal catalysts," in *Advances in Catalysis*, ed C. Song (Cambridge, MA: Academic Press Inc.), 1–35. doi: 10.1016/bs.acat.2017.10.001

Mondloch, J. E., Bayram, E., and Finke, R. G. (2012). A review of the kinetics and mechanisms of formation of supported-nanoparticle heterogeneous catalysts. *J. Mol. Catal. A Chem.* 355, 1–38. doi: 10.1016/j.molcata.2011.11.011

Mörke, W., Lamber, R., Schubert, U., and Breitscheidel, B. (1994). Metal complexes in inorganic matrixes. 11. Composition of highly dispersed bimetallic Ni, Pd alloy particles prepared by sol-gel processing: electron microscopy and FMR study. *Chem. Mater.* 6, 1659–1666. doi: 10.1021/cm00046a018

Mukainakano, Y., Li, B., Kado, S., Miyazawa, T., Okumura, K., Miyao, T., et al. (2007). Surface modification of Ni catalysts with trace Pd and Rh for oxidative steam reforming of methane. *Appl. Catal. A Gen.* 318, 252–264. doi: 10.1016/j.apcata.2006.11.017

Murphy, J. M., and Erkey, C. (1997). Copper(II) removal from aqueous solutions by chelation in supercritical carbon dioxide using fluorinated-diketones. *Ind. Eng. Chem. Res.* 36, 5371–5376. doi: 10.1021/ie970458i

Nashner, M. S., Frenkel, A. I., Adler, D. L., Shapley, J. R., and Nuzzo, R. G. (1997). Structural characterization of carbon-supported platinum–ruthenium nanoparticles from the molecular cluster precursor $PtRu_5C(CO)_{16}$. *J. Am. Chem. Soc.* 119, 7760–7771. doi: 10.1021/ja971039f

Negre, C. F. A., and Sánchez, C. G. (2013). "Optical properties of metal nanoclusters from an atomistic point of view," in *Metal Clusters and Nanoalloys: From Modeling to Applications*, eds M. M. Mariscal, O. A. Oviedo, and E. P. M. Leiva (New York, NY: Springer New York), 105–157. doi: 10.1007/978-1-4614-3643-0_4

Oviedo, O. A., and Leiva, E. P. M. (2013). "Thermodynamic modeling of metallic nanoclusters," in *Metal Clusters and Nanoalloys*, eds M. M. Mariscal, O. A. Oviedo, and E. P. M. Leiva (New York, NY: Springer), 305–350. doi: 10.1007/978-1-4614-3643-0_10

Özbakir, Y., and Erkey, C. (2015). Experimental and theoretical investigation of supercritical drying of silica alcogels. *J. Supercrit. Fluids* 98, 153–166. doi: 10.1016/j.supflu.2014.12.001

Özbakir, Y., Jonáš, A., Kiraz, A., and Erkey, C. (2017). Total internal reflection-based optofluidic waveguides fabricated in aerogels. *J. Sol-Gel Sci. Technol.* 84, 522–534. doi: 10.1007/s10971-017-4426-8

Pan, Y., Sun, K., Liu, S., Cao, X., Wu, K., Cheong, W. C., et al. (2018). Core-shell ZIF-8@ZIF-67-derived CoP nanoparticle-embedded N-doped carbon nanotube hollow polyhedron for efficient overall water splitting. *J. Am. Chem. Soc.* 140, 2610–2618. doi: 10.1021/jacs.7b12420

Patra, K. K., and Gopinath, C. S. (2016). Bimetallic and plasmonic Ag–Au on TiO_2 for solar water splitting: an active nanocomposite for entire visible-light-region absorption. *ChemCatChem* 8, 3294–3311. doi: 10.1002/cctc.201600937

Pekala, R. W. (1989). Organic aerogels from the polycondensation of resorcinol with formaldehyde. *J. Mater. Sci.* 24, 3221–3227. doi: 10.1007/BF01139044

Pierre, A. C., and Pajonk, G. M. (2002). Chemistry of aerogels and their applications. *Chem. Rev.* 102, 4243–4265. doi: 10.1021/cr0101306

Pinna, F. (1998). Supported metal catalysts preparation. *Catal. Today* 41, 129–137. doi: 10.1016/S0920-5861(98)00043-1

Pirzada, T., Ashrafi, Z., Xie, W., and Khan, S. A. (2019). Cellulose silica hybrid nanofiber aerogels: from sol-gel electrospun nanofibers to multifunctional aerogels. *Adv. Funct. Mater.* 30:1907359. doi: 10.1002/adfm.201907359

Raj kumar, T., Gnana kumar, G., and Manthiram, A. (2019). Biomass-derived 3D carbon aerogel with carbon shell-confined binary metallic nanoparticles in CNTs as an efficient electrocatalyst for microfluidic direct ethylene glycol fuel cells. *Adv. Energy Mater.* 9, 1–12. doi: 10.1002/aenm.201803238

Rao, C. R. K., and Trivedi, D. C. (2005). Chemical and electrochemical depositions of platinum group metals and their applications. *Coord. Chem. Rev.* 249, 613–631. doi: 10.1016/j.ccr.2004.08.015

Rechberger, F., and Niederberger, M. (2017). Synthesis of aerogels: from molecular routes to 3-dimensional nanoparticle assembly. *Nanoscale Horiz.* 2, 6–30. doi: 10.1039/C6NH00077K

Reetz, M. T. (2007). "Size-selective synthesis of nanostructured metal and metal oxide colloids and their use as catalysts," in *Nanoparticles and Catalysis*, ed A. Didier (Weinheim: Wiley-VCH Verlag GmbH & Co. KGaA), 253–277. doi: 10.1002/9783527621323

Rosseler, O., Shankar, M. V., Du, M. K., Schmidlin, L., Keller, N., and Keller, V. (2010). Solar light photocatalytic hydrogen production from water over Pt and Au/TiO_2 (anatase/rutile) photocatalysts: influence of noble metal and porogen promotion. *J. Catal.* 269, 179–190. doi: 10.1016/j.jcat.2009.11.006

Sadrieyeh, S., and Malekfar, R. (2018a). Mesoporous plasmonic nanocomposites based on Au/Ag-TiO_2 aerogels as SERS substrates. *Appl. Opt.* 57, 10510–10516. doi: 10.1364/AO.57.010510

Sadrieyeh, S., and Malekfar, R. (2018b). Photocatalytic performance of plasmonic Au/Ag-TiO_2 aerogel nanocomposites. *J. Non Cryst. Solids* 489, 33–39. doi: 10.1016/j.jnoncrysol.2018.03.020

Sahin, I., Özbakir, Y., Inönü, Z., Ulker, Z., and Erkey, C. (2017). Kinetics of supercritical drying of gels. *Gels* 4:E3. doi: 10.3390/gels4010003

Sahin, I., Uzunlar, E., and Erkey, C. (2019). Investigation of kinetics of supercritical drying of alginate alcogel particles. *J. Supercrit. Fluids* 146, 78–88. doi: 10.1016/j.supflu.2018.12.019

Sankar, M., Dimitratos, N., Miedziak, P. J., Wells, P. P., Kiely, C. J., and Hutchings, G. J. (2012). Designing bimetallic catalysts for a green and sustainable future. *Chem. Soc. Rev* 41, 8099–8139. doi: 10.1039/c2cs35296f

Sanli, D., and Erkey, C. (2013). Monolithic composites of silica aerogels by reactive supercritical deposition of hydroxy-terminated poly(dimethylsiloxane). *ACS Appl. Mater. Interfaces* 5, 11708–11717. doi: 10.1021/am403200d

Sanli, D., and Erkey, C. (2015). Silylation from supercritical carbon dioxide: a powerful technique for modification of surfaces. *J. Mater. Sci.* 50, 7159–7181. doi: 10.1007/s10853-015-9281-9

Sarac Oztuna, F. E., Barim, S. B., Bozbag, S. E., Yu, H., Aindow, M., Unal, U., et al. (2017). Graphene aerogel supported Pt electrocatalysts for oxygen reduction reaction by supercritical deposition. *Electrochim. Acta* 250, 174–184. doi: 10.1016/j.electacta.2017.08.067

Sarapuu, A., Samolberg, L., Kreek, K., Koel, M., Matisen, L., and Tammeveski, K. (2015). Cobalt- and iron-containing nitrogen-doped carbon aerogels as non-precious metal catalysts for electrochemical reduction of oxygen. *J. Electroanal. Chem.* 746, 9–17. doi: 10.1016/j.jelechem.2015.03.021

Schubert, U. (1996). New materials by sol-gel processing: design at the molecular level. *J. Chem. Soc. Dalt. Trans.* 90, 3343–3348. doi: 10.1039/DT9960003343

Smirnova, A., Dong, X., Hara, H., Vasiliev, A., and Sammes, N. (2005). Novel carbon aerogel-supported catalysts for PEM fuel cell application. *Int. J. Hydrogen Energy* 30, 149–158. doi: 10.1016/j.ijhydene.2004.04.014

Stamenkovic, V. R., Fowler, B., Mun, B. S., Wang, G., Ross, P. N., Lucas, C. A., et al. (2007). Improved oxygen reduction activity on $Pt_3Ni(111)$ via increased surface site availability. *Science* 315, 493–497. doi: 10.1126/science.1135941

Susanti, R. F., Kim, J., and Yoo, K. (2014). "Supercritical water gasification for hydrogen production: current status and prospective of high-temperature operation," in *Supercritical Fluid Technology for Energy and Environmental Applications*, eds V. Anikeev and M. Fan (Amsterdam: Elsevier B.V.), 111–137. doi: 10.1016/B978-0-444-62696-7.00006-X

Takanabe, K., Nagaoka, K., Nariai, K., and Aika, K. I. (2005). Titania-supported cobalt and nickel bimetallic catalysts for carbon dioxide reforming of methane. *J. Catal.* 232, 268–275. doi: 10.1016/j.jcat.2005.03.011

Tang, S., Vongehr, S., Wang, Y., Cui, J., Wang, X., and Meng, X. (2014). Versatile synthesis of high surface area multi-metallic nanosponges allowing control over nanostructure and alloying for catalysis and sers detection. *J. Mater. Chem. A* 2, 3648–3660. doi: 10.1039/C3TA14541G

Tesfaye, R. M., Das, G., Park, B. J., Kim, J., and Yoon, H. H. (2019). Ni-Co bimetal decorated carbon nanotube aerogel as an efficient anode catalyst in urea fuel cells. *Sci. Rep.* 9, 1–9. doi: 10.1038/s41598-018-37011-w

Thirumalraj, B., Rajkumar, C., Chen, S. M., Veerakumar, P., Perumal, P., and Liu, S., Bin (2018). Carbon aerogel supported palladium-ruthenium nanoparticles for electrochemical sensing and catalytic reduction of food dye. *Sens. Actuator B Chem.* 257, 48–59. doi: 10.1016/j.snb.2017.10.112

Tsang, C. H. A., Hui, K. N., and Hui, K. S. (2017). Electrooxidation of glucose by binder-free bimetallic Pd_1Pt_x/graphene aerogel/nickel foam composite electrodes with low metal loading in basic medium. *Electrochim. Acta* 258, 371–379. doi: 10.1016/j.electacta.2017.11.064

Tsang, C. H. A., Hui, K. N., and Hui, K. S. (2019). Influence of Pd_1Pt_x alloy NPs on graphene aerogel/nickel foam as binder-free anodic electrode for electrocatalytic ethanol oxidation reaction. *J. Power Sources* 413, 98–106. doi: 10.1016/j.jpowsour.2018.12.019

Tsang, C. H. A., and Leung, D. Y. C. (2017). Pd-Pt loaded graphene aerogel on nickel foam composite as binder-free anode for a direct glucose fuel cell unit. *Solid State Sci.* 71, 123–129. doi: 10.1016/j.solidstatesciences.2017.07.014

Tsang, C. H. A., and Leung, D. Y. C. (2018). Use of Pd-Pt loaded graphene aerogel on nickel foam in direct ethanol fuel cell. *Solid State Sci.* 75, 21–26. doi: 10.1016/j.solidstatesciences.2017.11.005

Türk, M., and Erkey, C. (2018). Synthesis of supported nanoparticles in supercritical fluids by supercritical fluid reactive deposition: current state, further perspectives and needs. *J. Supercrit. Fluids* 134, 176–183. doi: 10.1016/j.supflu.2017.12.010

Ulker, Z., Erucar, I., Keskin, S., and Erkey, C. (2013). Novel nanostructured composites of silica aerogels with a metal organic framework. *Microporous Mesoporous Mater.* 170, 352–358. doi: 10.1016/j.micromeso.2012.11.040

Vallribera, A., and Molins, E. (2008). "Aerogel supported nanoparticles in catalysis," in *Nanoparticles and Catalysis*, ed D. Astruc (Weinheim: Wiley-VCH Verlag GmbH & Co. KGaA), 161–194. doi: 10.1002/9783527621323.ch5

Vanrysselberghe, V., and Froment, G. F. (1996). Hydrodesulfurization of dibenzothiophene on a $CoMo/Al_2O_3$ catalyst: Reaction network and kinetics. *Ind. Eng. Chem. Res.* 35, 3311–3318. doi: 10.1021/ie960099b

Vu, H., Gonçalves, F., Philippe, R., Lamouroux, E., Corrias, M., Kihn, Y., et al. (2006). Bimetallic catalysis on carbon nanotubes for the selective hydrogenation of cinnamaldehyde. *J. Catal.* 240, 18–22. doi: 10.1016/j.jcat.2006.03.003

Walter, M. G., Warren, E. L., McKone, J. R., Boettcher, S. W., Mi, Q. X., Santori, E. A., et al. (2010). Solar water splitting cells. *Chem. Rev.* 110, 6446–6473. doi: 10.1021/cr1002326

Wang, D., and Zhu, Y. (2018). An effective Pt-Cu/SiO_2 catalyst for the selective hydrogenation of cinnamaldehyde. *J. Chem.* 2018:5608243. doi: 10.1155/2018/5608243

Wang, Y., Su, Y., Wang, W., Fang, Y., Riffat, S. B., and Jiang, F. (2019). The advances of polysaccharide-based aerogels: Preparation and potential application. *Carbohydr. Polym.* 226:115242. doi: 10.1016/j.carbpol.2019.115242

Wang, Y., Zhang, B., Pan, W., Ma, H., and Zhang, J. (2017a). 3D porous nickel–cobalt nitrides supported on nickel foam as efficient electrocatalysts for overall water splitting. *ChemSusChem* 10, 4170–4177. doi: 10.1002/cssc.201701456

Wang, Y., Zou, L., Huang, Q., Zou, Z., and Yang, H. (2017b). 3D carbon aerogel-supported PtNi intermetallic nanoparticles with high metal loading as a durable oxygen reduction electrocatalyst. *Int. J. Hydrogen Energy* 42, 26695–26703. doi: 10.1016/j.ijhydene.2017.09.008

Wanjala, B. N., Luo, J., Loukrakpam, R., Fang, B., Mott, D., Njoki, P. N., et al. (2010). Nanoscale alloying, phase-segregation, and core–shell evolution of gold–platinum nanoparticles and their electrocatalytic effect on oxygen reduction reaction. *Chem. Mater.* 22, 4282–4294. doi: 10.1021/cm101109e

Watkins, J. J., and McCarthy, T. J. (1995). Polymer/metal nanocomposite synthesis in supercritical CO_2. *Chem. Mater.* 7, 1991–1994. doi: 10.1021/cm00059a001

Wei, S., Wu, D., Shang, X., and Fu, R. (2009). Studies on the structure and electrochemical performance of Pt/Carbon aerogel catalyst for direct methanol fuel cells. *Energy Fuels* 23, 908–911. doi: 10.1021/ef8006432

Wen, D., and Eychmüller, A. (2017). 3D assembly of preformed colloidal nanoparticles into gels and aerogels: function-led design. *Chem. Commun.* 53, 12608–12621. doi: 10.1039/c7cc03862c

Wiebenga, M. H., Kim, C. H., Schmieg, S. J., Oh, S. H., Brown, D. B., Kim, D. H., et al. (2012). Deactivation mechanisms of Pt/Pd-based diesel oxidation catalysts. *Catal. Today* 184, 197–204. doi: 10.1016/j.cattod.2011.11.014

Winkler, A., Ferri, D., and Hauert, R. (2010). Influence of aging effects on the conversion efficiency of automotive exhaust gas catalysts. *Catal. Today* 155, 140–146. doi: 10.1016/j.cattod.2008.11.021

Xie, Y., Cheng, J., Liu, H., Liu, J., Maitituersun, B., Ma, J., et al. (2019). Co-Ni alloy@carbon aerogels for improving the efficiency and air stability of perovskite solar cells and its hysteresis mechanism. *Carbon* 154, 322–329. doi: 10.1016/j.carbon.2019.08.015

Yu, P. J., Hsieh, C. C., Chen, P. Y., Weng, B. J., and Chen-Yang, Y. W. (2016). Highly active and reusable silica-aerogel-supported platinum-cobalt bimetallic catalysts for the dehydrogenation of ammonia borane. *RSC Adv.* 6, 112109–112116. doi: 10.1039/C6RA24249A

Yu, P. J., Lee, M. H., Hsu, H. M., Tsai, H. M., and Chen-Yang, Y. W. (2015). Silica aerogel-supported cobalt nanocomposites as efficient catalysts toward hydrogen generation from aqueous ammonia borane. *RSC Adv.* 5, 13985–13992. doi: 10.1039/C4RA14002H

Zhang, B., Wang, H., Zuo, Z., Wang, H., and Zhang, J. (2018). Tunable CoFe-based active sites on 3D heteroatom doped graphene aerogel electrocatalysts: via annealing gas regulation for efficient water splitting. *J. Mater. Chem. A* 6, 15728–15737. doi: 10.1039/C8TA05705B

Zhang, J., Li, H., Guo, P., Ma, H., and Zhao, X. S. (2016). Rational design of graphitic carbon based nanostructures for advanced electrocatalysis. *J. Mater. Chem. A* 4, 8497–8511. doi: 10.1039/C6TA01657J

Zhang, M., Chen, Y., Chen, B., Zhang, Y., Lin, L., Han, X., et al. (2019). Fabrication of a three-dimensional visible-light-driven Ag-AgBr/TiO_2/graphene aerogel composite for enhanced photocatalytic destruction of organic dyes and bacteria. *New J. Chem.* 43, 5088–5098. doi: 10.1039/C8NJ06057F

Zhang, W., Wu, Y., Qi, J., Chen, M., and Cao, R. (2017). A thin NiFe hydroxide film formed by stepwise electrodeposition strategy with significantly improved catalytic water oxidation efficiency. *Adv. Energy Mater.* 7, 1602547. doi: 10.1002/aenm.201602547

Zhang, Y., Cangul, B., Garrabos, Y., and Erkey, C. (2008). Thermodynamics and kinetics of adsorption of bis(2,2,6,6-tetramethyl-3,5-heptanedionato)(1,5-cyclooctadiene) ruthenium (II) on carbon aerogel from supercritical CO_2 solution. *J. Supercrit. Fluids* 44, 71–77. doi: 10.1016/j.supflu.2007.08.010

Zheng, G. P., Lu, X., and Han, Z. (2016). Synthesis and electro-magneto-mechanical properties of graphene aerogels functionalized with Co-Fe-P amorphous alloys. *Micromachines* 7, 1–8. doi: 10.3390/mi7070117

Zhou, Y., Cheng, X., Yen, C. H., Wai, C. M., Wang, C., Yang, J., et al. (2017). Synthesis of an excellent electrocatalyst for oxygen reduction reaction with supercritical fluid: graphene cellular monolith with ultrafine and highly dispersive multimetallic nanoparticles. *J. Power Sources* 347, 69–78. doi: 10.1016/j.jpowsour.2017.02.044

Zhu, H., Guo, Z., Zhang, X., Han, K., Guo, Y., Wang, F., et al. (2012). Methanol-tolerant carbon aerogel-supported Pt–Au catalysts for direct methanol fuel cell. *Int. J. Hydrog. Energy* 37, 873–876. doi: 10.1016/j.ijhydene.2011.04.032

Conflict of Interest: The authors declare that the research was conducted in the absence of any commercial or financial relationships that could be construed as a potential conflict of interest.